Chapter 6

Interferometric Synthetic Aperture Radar (IFSAR)

Scott Hensley, Riadh Munjy, and Paul Rosen

TECHNOLOGY OVERVIEW

The last two decades has seen the development from initial concept to commercial systems of a mapping technology based on interferometric synthetic aperture radar (SAR). Conventional SAR has been used extensively since its inception in the late 1950's for fine resolution mapping and remote sensing applications [Elachi, 1988]. Operating at microwave frequencies (3-40,000 MHz) these systems are used to generate imagery that provides a unique look at the electromagnetic and structural properties of the surface being imaged, at day or night and in nearly all weather conditions. Conventional SAR systems typically measure only two image coordinates. One coordinate is measured along an axis oriented parallel to the flight direction while the other coordinate is the range (or distance) from the SAR to the point being imaged. By augmenting a conventional SAR system to have two spatially separated antennas in the cross-track plane it is possible to measure the three dimensional location of imaged points to a high degree of accuracy. Measurement of the third coordinate is based on an interferometric technique developed in the radio astronomy community over several decades for fine angular measurements. Combining of SAR and interferometry techniques into a single system is called interferometric synthetic aperture radar (IFSAR or sometimes referred to as InSAR or ISAR).

The main objectives of this chapter are to provide DEM users with an overview of how SAR and IFSAR systems work, what are the advantages and disadvantages of such systems, and to give users practical information regarding the collection, processing and quality assessment of data collected using IFSAR systems. Because many DEM users are not very familiar with SAR and IFSAR systems, this chapter includes a general overview of such systems in slightly greater detail than that found in other chapters. This overview will concentrate on the geometric aspects of SAR data collection and processing that are necessary for understanding IFSAR fundamentals. Readers interested in more of the hardware, system engineering or signal processing aspects of SAR are recommended to consult [Kovaly, 1976], [Curlander and McDonough, 1991].

Basic Concept

As with many surveying or mapping techniques IFSAR determines the location of a point in three dimensions by solving for an unknown component of a triangle associated to the observation geometry. The observation triangle in standard stereoscopic observations for determining topography is formed from two spatially separated viewing positions and a common point imaged from both vantages. Traditional stereoscopic measurement of the 'parallax' or relative displacement that an object has from two stereo images is proportional to the height of the object and to the separation between the two imaging points [Leberl, 1990]. For SAR systems the parallax is the range difference from a point to the two observing antennas. Useful topography measurements are possible when the observed parallax is measurable for height variations of interest. IFSAR allows measurements of parallax and consequent solution of the observation triangle for geometric conditions that would normally be considered degenerate.

The key to extending the range of useful stereoscopic observations is that parallax measurements are obtained by measuring the phase difference between signals received by the two IFSAR antennas. Distance measurements are related to phase measurements by converting the distance to units of wavelength and recalling each wavelength corresponds to 2π radians or 360° of phase. Explicitly, if $\Delta\rho$ is the distance, and λ is the wavelength of the microwave radiation, then the phase, ϕ, is given by

$$\phi = \underbrace{2\pi}_{\text{Radians per wavelength}} \underbrace{\frac{\Delta\rho}{\lambda}}_{\text{Number of wavelengths}} \qquad (6.1)$$

which is illustrated in Figure 6.1. Phase measurements in interferometric systems can be made with degree level accuracy, and with typical wavelengths in the range of 3-20 cm, corresponds to parallax measurements having millimeter to centimeter accuracy. This is in sharp contrast to the standard stereoscopic approach where the accuracy of the parallax measurement is usually on the order of the resolution of the imagery (several meters or more).
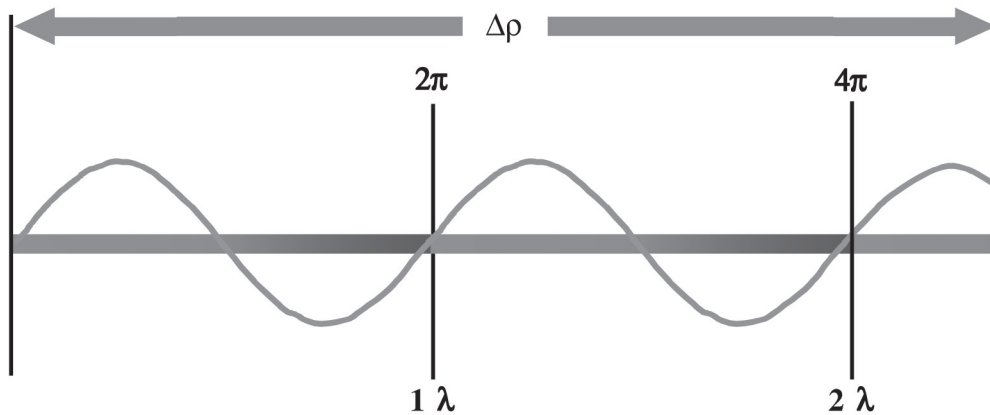

Figure 6.1 Figure illustrating the relationship between phase, distance and wavelength. See color plate in Appendix C.

Introduction to SAR

Before proceeding directly to IFSAR concepts and systems, a brief introduction to SAR systems and terminology is provided. Synthetic aperture radar can be used to produce high resolution imagery from either airborne or spaceborne platforms [Raney, 1999]. Unlike optical sensors operating at wavelengths between 3nm-30μm, such as photogrammetric or hyperspectral systems that form images from reflected solar radiation, SAR systems transmit their own radiation and record the signals reflected from the terrain. With optical systems images are generally formed instantaneously[1] whereas for SAR, data collected from multiple points along the flight path are required in order to achieve useful resolution in the along track, or azimuth, direction. Rather sophisticated image processing is required to form recognizable images from the raw data. The resolution and quality of the imagery depends on a number of system parameters as well as how the data are collected and processed.

---

[1] Exceptions include scanning optical systems such as Landsat where the optics are scanned and the image is generated one line (or pixel) at a time. This is not a fundamental sensor constraint, that is if adequate lenses and optical recording technology are available then a full two dimensional image could be made instantaneously.

SAR takes advantage of the motion of the platform to synthesize a large antenna that may be many hundreds of meters in length to achieve fine along track resolution. Figure 6.2 shows the typical SAR imaging geometry with the SAR platform moving along in flight. The radar antenna points in a direction perpendicular to the flight path called the range or cross track direction imaging the terrain below. At approximately regular intervals along the flight path the radar transmits a signal called a pulse and then records the returned echo.
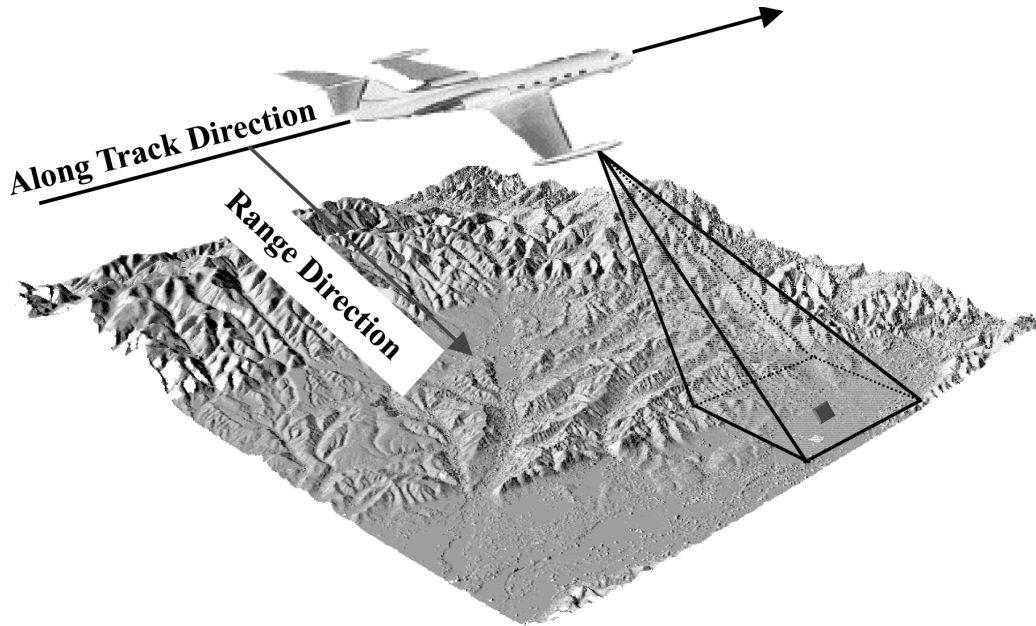

Figure 6.2 A typical SAR imaging geometry has a platform containing a radar instrument moving in the along track direction and imaging the terrain to one side of the flight path. The SAR transmits a series of pulses at regular intervals along track that simultaneously illuminates an area in the along track direction much greater than the desired azimuth resolution. By recording the returned echo from each pulse and using signal processing techniques to "synthesize" a larger antenna, fine resolution in azimuth is achieved. The blue square in the center of beam shows the size of a resolution element compared with the illuminated area from a single pulse indicated in green. See color plate in Appendix C.

Range or cross track resolution is achieved by finely gating the received echo in time. Nominally, range resolution is limited by the width of the transmitted pulse because energy returned from any point of a pulse cannot be distinguished from another point within the pulse. For systems that transmit ultra-narrow pulses, no additional processing in range is required. Many operational systems find it impractical to transmit such narrow pulses due to peak power limitations or other hardware considerations. In order to reduce the peak power in a transmitted pulse yet maintain the same average power, it is desirable to have longer pulses without somehow sacrificing range resolution. This is achieved by encoding the transmitted pulse in such a way as to be able to distinguish where within a pulse the returned energy originated. The method used by many airborne platforms is chirp encoding where the frequency is linearly changed across the pulse as illustrated in Figure 6.3. The amount of frequency variation across a pulse is called the range bandwidth. Range resolution is inversely proportional to the bandwidth. For coded pulses the desired range resolution is achieved only after a signal processing step called range compression. Table 6.1 shows the conversion between range resolution and bandwidth for a wide range of currently operational SAR systems.
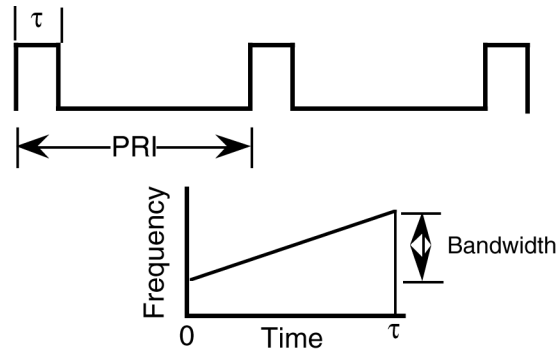
Figure 6.3 The radar emits a sequence of pulses separated in time. The time duration between pulses is called the interpulse period (IPP) and the associated pulse frequency is called the pulse repetition frequency (PRF=1/IPP). The pulse duration, τ, is called the pulse length. For many radars, each pulse is frequency encoded with a linear frequency ramp across the pulse known as a chirp.

Table 6.1 Bandwidth to resolution table.

Bandwidth (MHz)	Resolution (m)
400	.37
300	.5
160	.95
80	1.9
40	3.7
20	7.5
10	15.0

Azimuth resolution is achieved by synthesizing a large antenna from the echoes received from a sequence of pulses illuminating a target. Without signal processing the intrinsic azimuth resolution from a single transmitted pulse would be the azimuth angular width of the antenna beam times the range, that is the width the antenna footprint on the ground. By combining the echoes using appropriate signal processing algorithms from all the pulses imaging a point, the azimuth resolution is dramatically improved. Azimuth resolution after processing is determined by the size of the synthetic aperture (or antenna), which is the length of flight track over which a fixed point stays within the azimuth antenna beamwidth. The beamwidth of an antenna, θ_{bw}, is given by

$$\theta_{bw} = k\frac{\lambda}{L} \tag{6.2}$$

where λ is the wavelength, L is the physical antenna length, and k is a constant that depends on the antenna (typically between .8 and 1.5). The size of the antenna footprint on the ground in the azimuth direction is approximately given by

$$l_{az} = \rho\theta_{bw} = \rho\frac{\lambda}{L} \tag{6.3}$$

144   Chapter 6

where ρ is the range to a point in the footprint as is depicted in Figure 6.4. This is the synthetic aperture length.
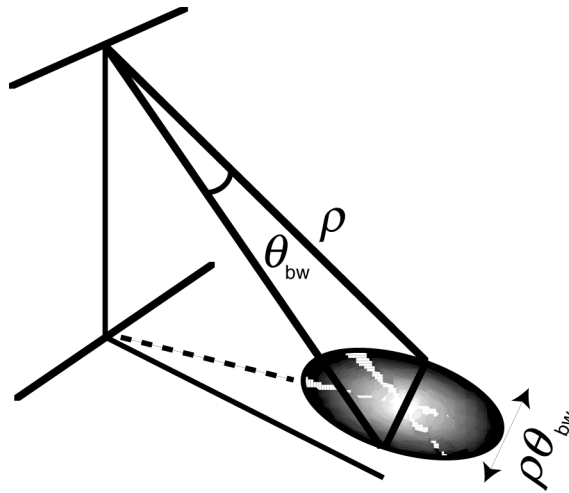

Figure 6.4 Figure showing the antenna footprint size in the azimuth direction depends on the range and the antenna beamwidth in the azimuth direction.

Since the length of the synthetic aperture is much longer than the actual antenna mounted on the SAR platform, Equation 6.2 indicates that if we were to replace the actual antenna length with the synthetic aperture length we should achieve a much narrower beamwidth, and therefore finer azimuth resolution. The process of forming the synthetic aperture to achieve the increased azimuth resolution is called azimuth compression.

During the time a target is in the beam, the range to the target is changing from pulse-to-pulse. After generating a SAR image we identify a target's location in the image by its azimuth and range position as shown in Figure 6.5. To select a unique range from the family of ranges that are changing from pulse-to-pulse during the synthetic aperture, the angle from the velocity vector to the target (or equivalently the Doppler frequency[2]) is specified for processing as shown in Figure 6.6.
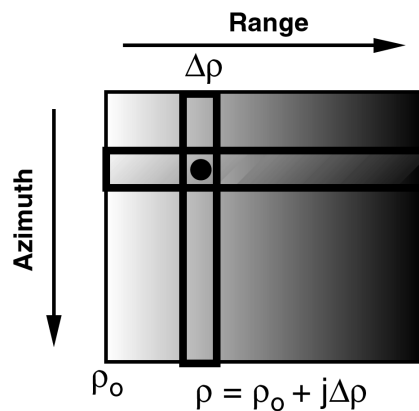

Figure 6.5 Shown above is a target imaged in the jth range bin.

[2] Doppler frequency is the shift in frequency that occurs when a transmitter and receiver are in relative motion. The Doppler frequency shift is a function of the angle between the relative velocity vector and line-of-sight between transmitter and receiver and the wavelength. SAR processors typically specify the Doppler frequency to coincide with where the antenna is pointing to get maximal signal strength.

Chapter 6   145

The bold dashed line from pulse N-2 to the target indicates the desired Doppler (or equivalently angle) at which the target will be imaged. Observe that selection of the Doppler frequency not only affects the range at which a target is imaged but the corresponding position of the platform (and hence azimuth location) when the target is imaged.
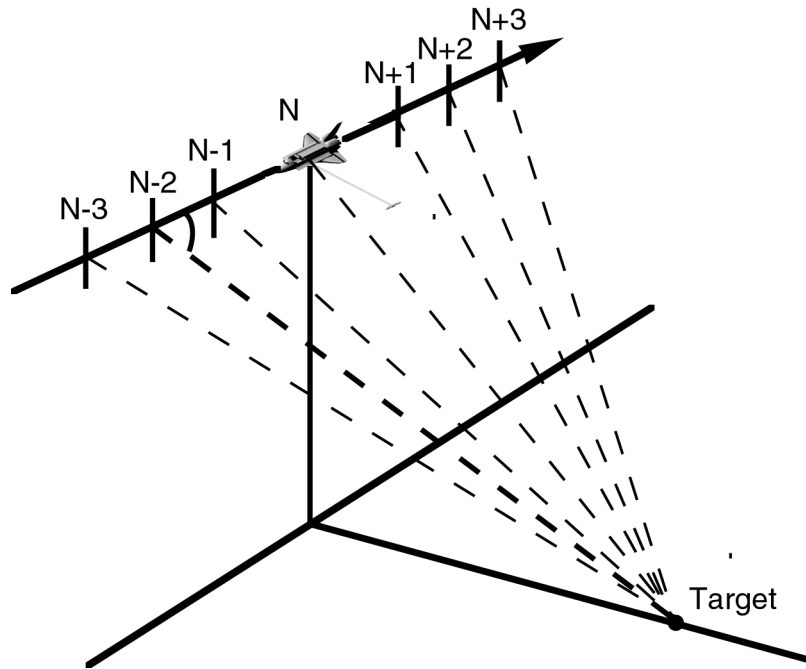

Figure 6.6 This figure shows the shuttle imaging a fixed point on the ground from a number of pulses in a synthetic aperture. The range at which a target appears in a synthetic aperture image depends on the processing parameters and algorithm used to generate the image. For standard range/Doppler processing the range is fixed by choosing the pulse which has a user defined fixed angle between the velocity vector and the line-of-sight vector to the target. This is equivalent to selecting the Doppler frequency.

It is useful for our subsequent discussion of IFSAR systems to distill the above information on SAR image coordinates to the simple geometry of the intersection of two surfaces. As discussed earlier, range information is obtained by measuring the time it takes a radar pulse to propagate from the antenna to a target and return. Azimuth location is determined from the Doppler frequency shift that is related to the angle from the velocity vector when a target is imaged. Viewing SAR target location geometrically, the range/azimuth location locus is the intersection of a sphere centered at the antenna with radius equal to the radar range and a cone with generating axis along the velocity vector with cone angle proportional to the Doppler frequency as shown in Figure 6.7. A target in the radar image could be located anywhere on the intersection locus which is a circle in the plane formed by the radar line of sight to the target and vector pointing from the aircraft to nadir. Since the intersection is a curve in three dimensional space, further information is required in order to locate a target uniquely.

Because the range direction is not parallel to ground coordinates as shown in Figure 6.8, SAR images are distorted relative to a planimetric view. In many applications this distortion can adversely affect data interpretation, particularly when one is not well acquainted with SAR imagery [Leberl, 1990]. IFSAR systems, being able to resolve the three dimensional coordinates of points in SAR imagery, can produce imagery having correct planimetric placement in regions where there are good interferometric phase measurements. These corrected images are often easier to interpret and
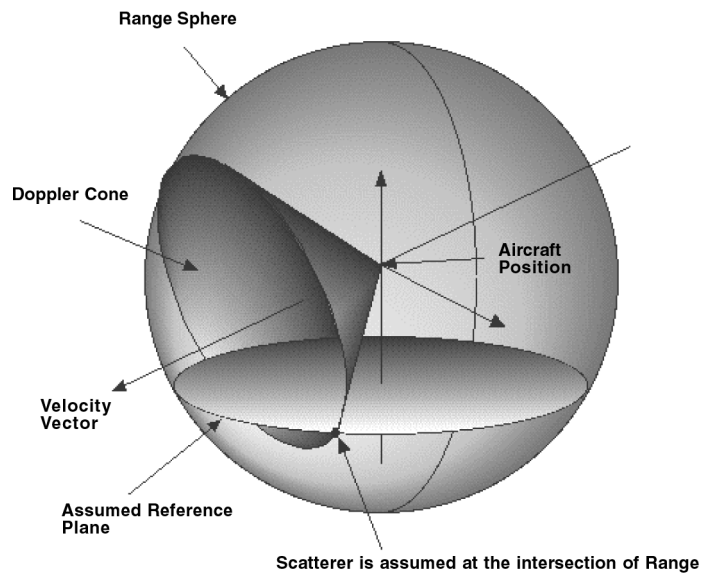
Figure 6.7 Figure showing the geometric view of target location in SAR imagery. Range information locates a target on a sphere centered about the SAR platform and the Doppler frequency locates a target on a cone centered about the velocity vector. The intersection locus of these two surfaces is a circle and thus the three dimensional location of a target cannot be uniquely determined from a single image.

are easier to register with other data layers required for analysis. Three common features observed in SAR imagery that bear particular mention are foreshortening, layover and shadow.

Foreshortening in radar imagery results from the fact that relief displacement is towards the direction of the radar. Because the range increases more slowly than ground coordinates on slopes facing toward the radar (higher elevations contend with increasing ground distance, slowing the range increase) they tend to appear bunched relative to a planimetric view. The opposite occurs on slopes facing away from the radar (lower elevations coupled with increasing ground distance speeds the range increase) where they tend to expand out when compared to a planimetric view. Both situations are illustrated in Figure 6.8. Note that foreshortening in radar images is opposite to that of optical imagery where relief displacement is away from the direction of the camera.

Layover is a limiting case of foreshortening where points arranged with increasing ground coordinates appear reversed in the radar imagery. Layover occurs because the range to objects with larger ground coordinates is less than the range to other objects with smaller ground coordinates. Geometrically this happens when the slope of the terrain is greater than the angle the incident radiation makes with respect to vertical. More importantly for our purposes is to note for interferometric radar systems layover causes a loss of useful signal and therefore precludes the determination of elevation in layover regions.

Shadow occurs when the radar beam cannot reach a portion of the terrain being imaged because it is occulted by other parts of the terrain or other objects in the scene. Where the terrain is shadowed the radar image will appear dark and the signal in these range cells is only due to thermal noise. As with layover regions, shadowed regions have no useful interferometric signal and consequently no elevation values can be determined.

Synthetic aperture radar systems are currently operating over a wide range of frequencies and resolutions depending on their intended applications. Operating frequencies vary from as low as

Chapter 6

147

3 MHz to as high as 40 GHz. The choice of frequency is dictated by a number of factors including intended application, platform and power constraints, and availability of the desired frequency range. Table 6.2 shows the correspondence between frequency, wavelength and the band designation letter code (assigned in World War II for security reasons) that are often used to specify the operating frequency of the radar.
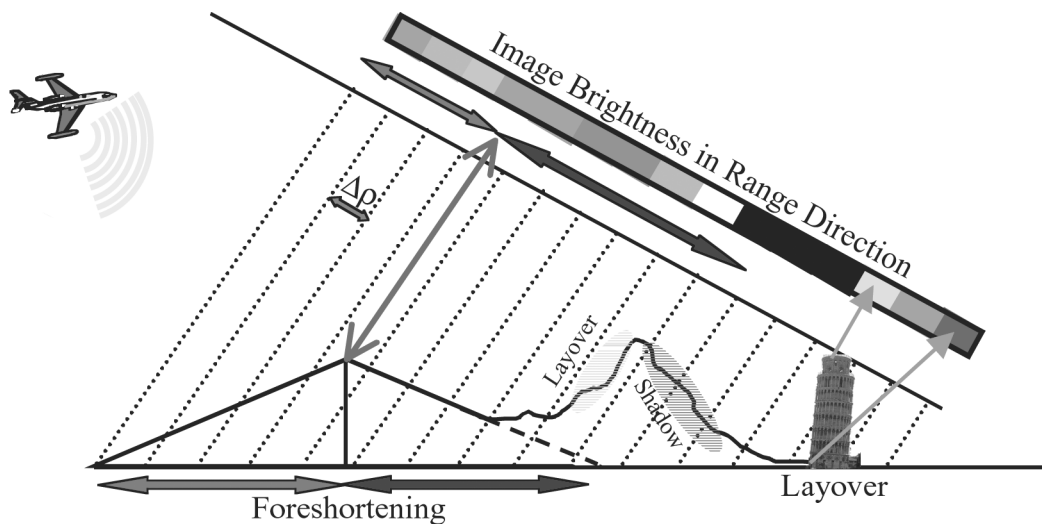

Figure 6.8 The three-dimensional world is collapsed to two dimensions in conventional SAR imaging. After image formation, the radar return is resolved into an image in range-azimuth coordinates. This figure shows a profile of the terrain at constant azimuth, with the radar flight track into the page. See color plate in Appendix C.

Table 6.2 Frequency and Wavelength Relationship Table.

Frequency Band (MHz)	Wavelength Range (cm)	Band Identification
26500-40000	1.13-.75	Ka
18000-26500	1.66-1.13	K
12500-18000	2.4-1.66	Ku
8000-12500	3.75-2.4	X
4000-8000	7.5-3.75	C
2000-4000	15-7.5	S
1000-2000	30-15	L
300-900	100-33	P or UHF
30-300	1000-100	VHF
3-30	10000-1000	HF

To appreciate why particular radar frequencies (wavelengths) are selected for a given application, it is necessary to have a cursory understanding of how radar signals interact with terrain [Elachi, 1988], [Raney, 1999]. Each pixel in a SAR image is a complex number having a magnitude and phase determined by the terrain surface properties and the image geometry. A radar signal impinging on a resolution element (area of the surface contained within a single range and azimuth bin) will in general scatter energy in all directions. The signal reflected back toward the radar is referred to as the backscatter. Backscatter strength is a function of the composition of the surface and its structure. Electrical composition of a surface is characterized by its dielectric constant. The dielectric constant of a material determines how much energy is absorbed or reflected from the surface and depends on the radar frequency. Surface structure is usually characterized by roughness, a measure of how much the surface varies in a resolution element. Roughness is measured in terms of the incident radiation's wavelength, so surfaces that are smooth at one wavelength may appear rough at another wavelength. As a general rule of thumb the rougher the surface the greater the backscatter. For example, a road that is relatively flat and free of potholes or other major imperfections may appear very smooth when imaged using a L-band (23 cm wavelength) radar because a typical road's micro-topography may be less than 5 mm. However, the same road imaged with a Ka-band (7.5 mm wavelength) radar may seem quite rough and appear bright in a radar image. Figure 6.9 illustrates in a qualitative sense how radar interacts with different types of ground cover, and Figure 6.10 shows the same area imaged at X and P-band with the GeoSAR radar.
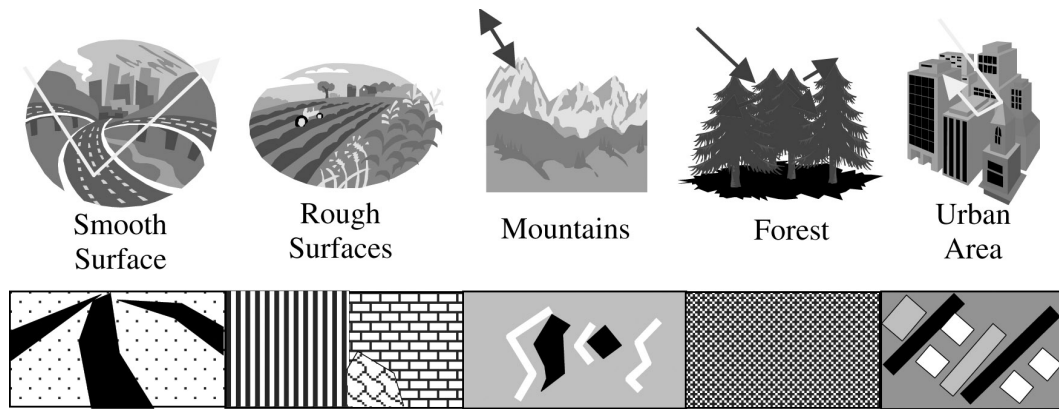

Figure 6.9 Above are five common ground cover types found in SAR imagery. Smooth surfaces such as roads or water tend to reflect energy away from the radar and appear dark in radar images. Rough surfaces, such as often found in fields and cropland, exhibit a type of checkerboard pattern of fields with the texture and brightness level varying with crop and field condition. Extremely bright lines running parallel to the look direction as a result of layover coupled with shadowed regions is typical of that found in mountainous regions. Forested areas generally appear relatively bright since the rough nature of the canopy at most wavelengths generates high levels of backscatter. Depending on the resolution of the SAR, urban areas can show individual buildings or groups of building and the associated roadways. See color plate in Appendix C.
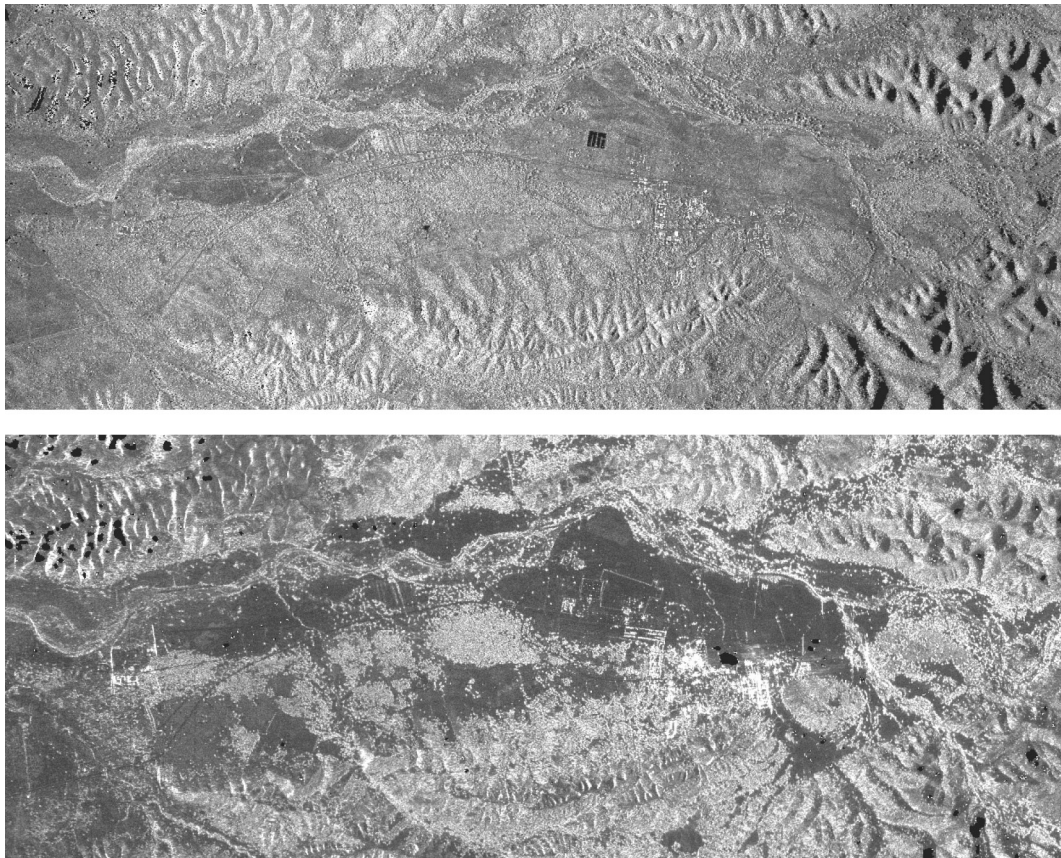
Figure 6.10 GeoSAR X-band (top) and P-band (bottom) orthorectified SAR images of Hunter Liggett. Notice how the vegetated areas in the center portion of the image have much greater contrast at P-band (85 cm wavelength) than X-band (3 cm wavelength). This contrast differential results from open areas appearing smoother at P-band than X-band whereas the vegetated areas appear rough at both wavelengths. In the hilly regions at the top-left and bottom-right portions of the image are some areas of shadow and layover.

Although the above discussion primarily concentrated on the observed magnitude in a SAR image, it is the phase that is needed for interferometry. The two primary components of the phase measurement consist of a systematic and a random part. The systematic part is the range to the resolution elemoment converted to phase modulo 2π. Even though there may be many millions of wavelengths (hence many multiples of 2π) from the antenna to a resolution element, only the principal value (a number between $-\pi$ and π) can be extracted from a complex-valued resolution element.

The random component is a result of a thermal noise contribution and the coherent sum of contributions from all the elemental scatterers in a resolution element. The elemental scatterers are points within a resolution element that dominate the signal value, and their contribution depends only on the viewing geometry and the composition of the scatterers. In general, because the distribution of elemental scatterers within a resolution element changes from element to element and the range converted to phase modulo 2π to a resolution element is randomly distributed, phase values in SAR images are randomly distributed. Because these effects cannot be separated, phase values from a single SAR image are generally ignored. It is important for the IFSAR discussion to follow to note that if the viewing geometry is nearly unchanged, and the elemental scatterers within a resolution cell are undisturbed, then this portion of the random phase remains the same. Thus the thermal noise is random in time and the scatterer noise is random in space.

Because radar primarily interacts with structures that have lengths comparable to the wavelength or larger, longer wavelength (lower frequency) radars tend to penetrate deeper into the vegetation canopy or ground surface. The amount of penetration in a vegetation canopy depends on the structure and density of the vegetation. Radar wavelengths less than roughly 10 cm mostly sense the upper portions of canopies while wavelengths longer than 20 cm sense deeper into a canopy. This differential penetration effect for lower frequency radars has led to the development of radar systems designed to exploit this phenomenon. Ground surface penetration depends on the type and composition of the ground layers, ground cover and soil moisture. Longer wavelength radars have been known to penetrate several meters or more in dry sandy soil and even deeper into certain types of ice.

IFSAR Overview

By augmenting a conventional SAR system with another spatially separated receiving antenna, as illustrated in Figure 6.11, it is possible to extract topographic information. More detail on IFSAR systems and processing can be found in [Rosen et al, 2000], [Madsen and Zebker, 1999], [Franceschetti, 1999] and [Bamler and Hartl, 1998]. While radar pulses are transmitted from the conventional SAR antenna, radar echoes are received by both the conventional and an additional SAR antenna. If the received signals from the two antennas are combined *coherently* for each imaged point to measure the phase difference, then the system forms an interferometric SAR. Here the interferometric phase difference is essentially related to the geometric path length difference to the image point, which depends on the topography. With knowledge of the interferometer geometry, the phase difference can be converted into an altitude for each image point. By having a third measurement, the interferometric phase, in addition to the standard along and cross track location of an image point obtained with conventional SARs, it is possible to determine the three-dimensional location of a point.

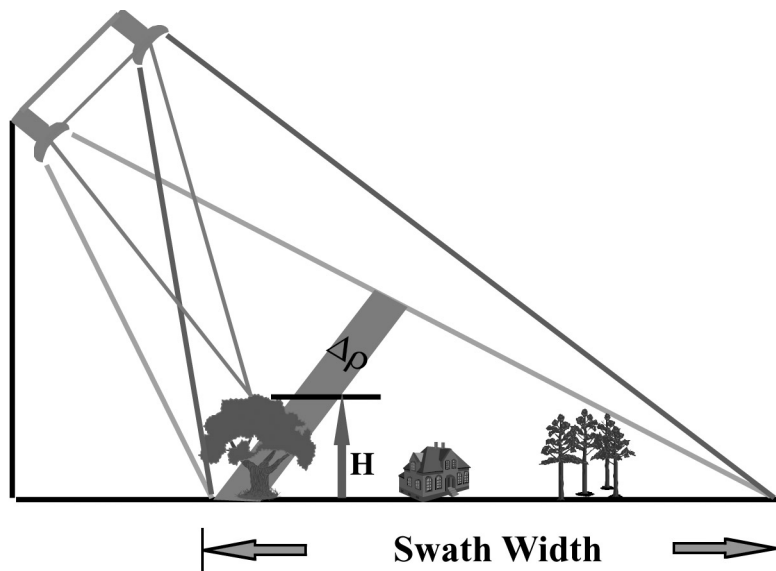
Figure 6.11 Interferometric SAR for topographic mapping uses two apertures separated by a "baseline" to image the surface. The phase difference between the apertures for each image point, along with the range and knowledge of the baseline, can be used to infer the precise shape of the imaging triangle (in red) to determine the topographic height of an object. See color plate in Appendix C.

Previously, it was shown that knowing the SAR coordinates of a target restricted its location to be on the intersection locus of a sphere and cone that from Figure 6.7 was seen to be a circle. Parameterizing the location on this circle by an angle, referred to as the elevation angle, θ, reduces the three dimensional target location problem to determining this angle. For this we need the interferometric measurement. Assume two identical antennas, A1 and A2, are receiving radar echo signals from a single source as shown in Figure 6.12.
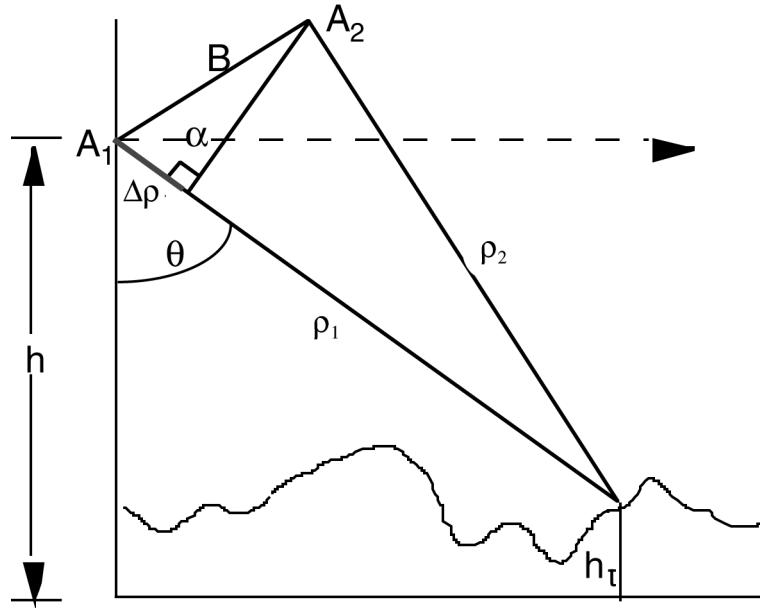

Figure 6.12 Simplified broadside looking (zero Doppler) radar interferometry geometry. The difference in range from the two observing antennas to the target is approximately equal to the projection of the baseline vector onto the line-of-sight vector shown in blue. This range difference can be related to a phase measurement using equation 6.1 and forms the primary interferometric observable. See color plate at Appendix C.

The path length difference, $\Delta\rho$, of the signals received by the two antennas is approximately given by

$$\Delta\rho = |\vec{\rho_1}| - |\vec{\rho_2}| \approx B\sin(\theta-\alpha) \tag{6.4}$$

where $\vec{\rho_i}$ indicates the vector from antenna 1 to the target, B is the length of the baseline vector which is the vector pointing from antenna 1 to antenna 2, θ is the desired elevation (or look) angle and the baseline orientation angle, α, is the angle the baseline vector makes with respect to the horizontal. Observe that the range difference to a good approximation for most systems is simply the length of the projection of the baseline vector onto the line-of-sight. The range difference, $\Delta\rho$, may be obtained by measuring ϕ, the phase between the two interferometer signals, using the relation

$$\phi = -\frac{2\pi m\Delta\rho}{\lambda} \quad m=1,2 \tag{6.5}$$

where λ is the radar wavelength and m equals 1 when the path length difference is associated with the one-way path difference, or 2 for the two-way path difference as is the case for Ping-Pong or repeat pass systems described below. Geometrically, the phase measurement provides a second cone with cone axis the interferometric baseline. Intersecting the phase cone with the range sphere and Doppler cone determines the elevation angle to the target and therefore the target's full three-dimensional location as shown in Figure 6.13.
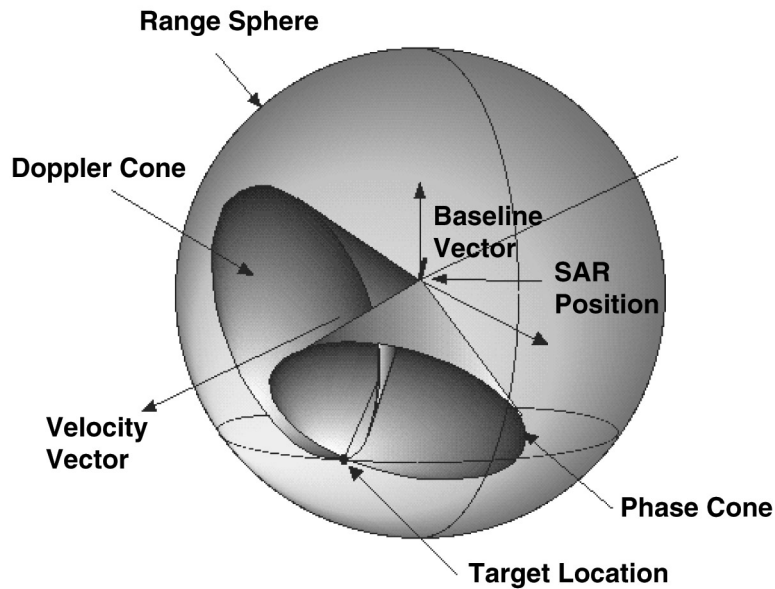
Range Sphere
Doppler Cone
Baseline Vector
SAR Position
Velocity Vector
Phase Cone
Target Location

Figure 6.13 Target location in a SAR image could be anywhere on the intersection of a range sphere and Doppler cone thereby providing no information on the target's elevation. 3-D information is obtained by the intersection of the phase cone with range sphere and Doppler Cone.

Using the simplified geometry of Figure 6.10 the height of a target, ht, is given by

$$h_t = h - \rho\cos(\theta) \tag{6.6}$$

where h is the altitude of the radar antenna and ρ is the slant range from the antenna to the target. Since the signal phase is sensitive to displacements between images of a fraction of a wavelength, the interferometric technique provides a very accurate means of determining topographic heights. Using Equations 6.4 and 6.5 the elevation angle can be determined to be

$$\theta = \sin^{-1}\left(\frac{\lambda\phi}{2\pi mB}\right) + \alpha \tag{6.7}$$

It is immediate from Equations 6.6 and 6.7 that determining the height of a target requires knowledge of the platform position, the range, the interferometric baseline length, the baseline angle and the interferometric phase. Generation of accurate topographic maps using radar interferometry places stringent requirements on the knowledge of the platform and baseline vectors. Figure 6.14 shows interferometric phase measurements and amplitude images.
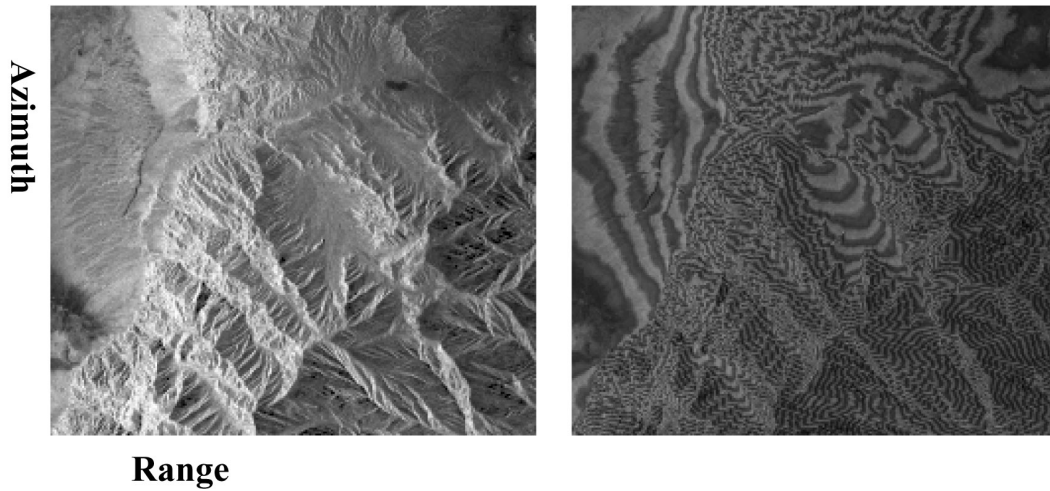
Azimuth

Range

Figure 6.14 Interferometric phase and associated amplitude image of the Mojave Desert, CA, generated from repeat pass observations using the SIR-C radar. See color plate in Appendix C.

Understanding conditions when interferometric phase measurements useful for topographic mapping are possible requires us to examine more closely what happens to radar signals within a resolution element. Consider a resolution cell with elemental scatterers arranged throughout as shown in Figure 6.15. Each elemental scatterer will contribute a portion of the backscatter that is added coherently with the other elemental scatterers to produce the return from the cell. Since the return from the elemental scatterers adds coherently, the relative phase or distance between the scatterers affects the magnitude and phase of the total signal. Conceptually, the phase can be decomposed into a systematic and random component by selecting the center of the cell as reference. The systematic component is the phase from the antenna to the center of the cell and is the portion of the signal needed for interferometry. The random component is the coherent sum of the signals from the randomly arranged elemental scatterers within the cell to the center of the cell. This component, although random from resolution element to resolution element, remains the same (or nearly the same) if the viewing geometry is nearly identical and if the relative position of the elemental scatterers within a cell remain the same (or nearly the same) as shown in Figure 6.15.
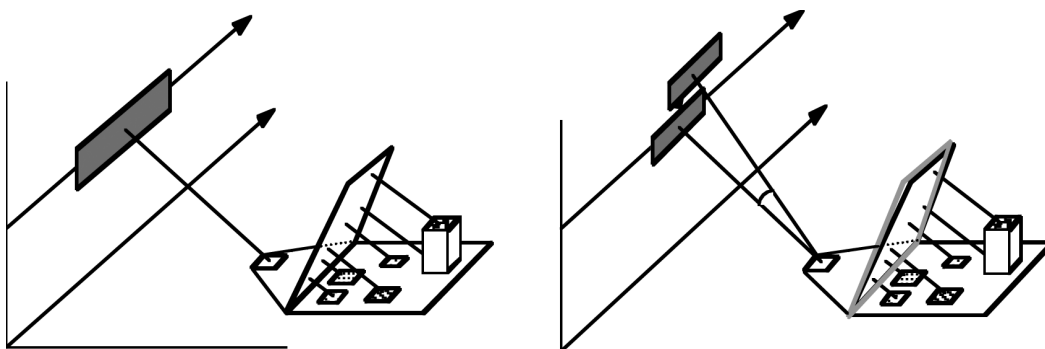
Figure 6.15 The left portion of the figure shows a notional arrangement of elemental scatterers within an imaging cell. Each elemental scatterer may have different surface roughness and dielectric properties as indicated by the different shading patterns. The right portion of the figure shows that if the imaging geometry is nearly the same the relative distance between scatterers is preserved and cancels out in the interferometric phase measurement.

For interferometric applications, where the viewing geometry of the interferometric pair is nearly the same, the random component arising from the elemental scatterer arrangement cancels and leaves only the difference between systematic components. This phase difference is the interferometric phase measurement and equals the phase in Equation 6.5 modulo 2π. Another random component, which does not cancel, is thermal noise. Thermal noise is different for each receiving antenna, and depending on its magnitude relative to the desired signal degrades interferometric phase measurement. The above discussion is summarized below.

phase = range from antenna to center of cell + Coherent sum of elemental scatterers arranged randomly in cell + thermal noise

Systematic component desired by interferometric measurement

Random component that if look direction is nearly the same and scatterers within cell do not move relative to each other this component cancels in the interferogram formation process.

Random component that does not cancel and results in interferometric phase noise

It is important to appreciate the consequences of the fact the interferometric phase measurement is made modulo 2π. The total range difference between the two observations that the phase represents in general can be many multiples of the radar wavelength, or expressed in terms of phase, many multiples of 2π. It is this value that is required in order to make height measurements. The standard approach for determining the unique phase that is directly proportional to the range difference is to first determine the relative phase between pixels via the so-called "phase unwrapping" process. Unwrapping of IFSAR imagery is a non-trivial process for which a number of algorithms have been developed. Complications arise in avoiding unwrapping errors in regions of shadow, layover and low signal return. The connected phase field after unwrapping may still need to be adjusted by an overall constant of 2π. The step that determines the overall constant of 2π is referred to as absolute phase determination.

Interferometric correlation, a measure of the similarity of the signal received at the two antennas, can be estimated directly from the image data of the two interferometric channels [Zebker and Villasenor, 1992]. Correlation measurements have values between 0 and 1, with 1 designating perfect correlation between the channels. Sometimes it is more convenient to refer to the amount of interferometric decorrelation, which is defined as one minus the correlation. The amount of decorrelation due to the slightly different viewing geometry is called geometric decorrelation. Thermal noise induced signal decorrelation is called noise decorrelation. Shadowed regions suffer from noise decorrelation and areas on steep slopes exhibit geometric decorrelation that increases phase noise and can preclude useful phase measurements altogether. Another form of decorrelation occurs when there is a vertical distribution of scattering elements within a resolution element as shown in Figure 6.16. Not only is the signal decorrelated, the point within the resolution cell corresponding to the interferometric phase measurement depends on the wavelength and the scatterer distribution in the cell. This form of decorrelation is called volumetric decorrelation and can be used to infer information about the vertical structure of the volume. Recently, there has been a great deal of activity using volumetric correlation to estimate tree and canopy structure within the interferometric SAR community.

Look Direction

$\Delta\rho$

$\Delta\rho$
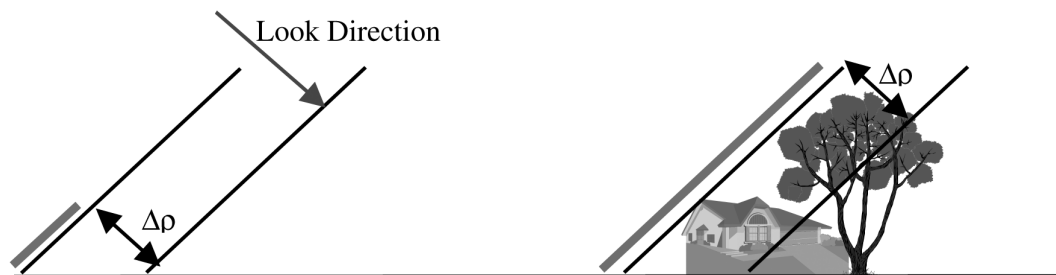
Figure 6.16 Vertical structure of scatterers within a resolution element due to vegetation or other structures present in the cell cause increased decorrelation. This form of decorrelation can be used to infer information about vertical structure within a resolution element. The increased decorrelation results from the increased size of the range cell projected back toward the direction of the radar (shown in magenta) when compared to a flat surface.

Chapter 6

155

There is an upper value on the useful baseline length known as the critical baseline [Rosen et al, 2000]. The critical baseline is reached when the amount of phase change per resolution element exceeds 2π radians. This limitation is a result of the fact that the interferometric phase measurement is made only modulo 2π. As the baseline approaches the critical baseline, the phase values from the two antennas become completely decorrelated. However, as the baseline increases, the sensitivity of phase to height increases improving the accuracy of interferometric SAR systems. Practical mapping systems must select baselines with a balance between adequate phase to height sensitivity to meet mapping requirements and excessive decorrelation with corresponding processing difficulties.

Combining the SAR image formation process, interferometric phase measurement, unwrapping and height determination into an automated processing algorithm has a process flow that is shown in Figure 6.17 [Madsen et al, 1993]. An understanding of the steps involved is useful for understanding IFSAR calibration and for identifying potential error sources in IFSAR generated DEMs. Raw data are collected and stored onboard for batch processing. The first processing step is decoding the byte data, followed by range compression for each of the two interferometric channels. Using the platform motion information obtained from Inertial Navigation System (INS) and Global Positioning System (GPS) measurements, as well as any other baseline metrology devices, the data are compensated for perturbations in aircraft motion from a reference path[3] and then azimuth compressed. This generates two single-look complex images.

One image of the single-look complex image pair is resampled to overlay the other. This registration must be done to a small fraction of a pixel (typically less than .1 of a pixel) in order to avoid phase decorrelation. Multiplying the complex pixel value in one image by the complex conjugate of the corresponding pixel value in the second image forms an interferogram. The resulting interferogram is multi-looked, by spatially averaging the complex pixels in a box about a given pixel to reduce the amount of phase noise.

Figure 6.17 Interferometric processing block diagram.

---

[3] The process of correction for motion away from an ideal path is referred to as motion compensation. Motion compensation corrects for motion on the order of fractions of a wavelength in order to generate well focused SAR imagery. The requirements for motion compensation are even more demanding for IFSAR systems and place stringent requirements on the platform and baseline metrology systems.

After the multi-looked interferogram has been generated the phase for each complex sample is computed. To generate a continuous height map, the two-dimensional phase field must be unwrapped. After the unwrapping process an overall multiple of 2π is estimated and added to the unwrapped phase (the estimated value may be 0).

Subsequent to determining the absolute phase for each pixel in the interferogram and possibly taking additional looks, the 3-dimensional target position can be determined. Phase corrections are applied to the interferometric phase to account for tropospheric effects, and the range is corrected to account for the speed of light changes in the atmosphere. Using accurate baseline and platform position information, the phase and range information for the target position is computed. A relief map is generated by gridding the unevenly sampled 3-dimensional target locations in a natural coordinate system aligned with the flight path. The gridded products include the target heights, the SAR image which has been orthorectified, a correlation map, and a height error map described below. These four products will be referred to as primary mapping or strip map products. The resulting radar relief map may be measuring the heights above the ground, within the vegetation canopy or beneath the surface, in arid regions. To convert this map into a true ground surface DEM corrections based on phenomenological studies, e.g. using scattering or semi-empirical curves to correct elevation measurements based on the amount of decorrelation in the canopy, must be incorporated into either the 3-dimensional location algorithms or into a post processing step.

One of the unique aspects of interferometric SAR systems is the ability to determine the statistical height error, that is the degree of height noise from pixel to pixel, estimated from knowledge of the correlation, γ [Hensley and Webb, 1994]. The amount of phase noise between the two channels is simply and directly related to the correlation and number of looks used to reduce phase noise[4]. The Cramer Rao bound relating the phase variance, σ_ϕ, to the correlation coefficient, γ, is given by

$$\sigma_\phi = \frac{1}{\sqrt{2N_L}}\frac{\sqrt{1-\gamma^2}}{\gamma} \tag{6.8}$$

where N_L is the number of looks. From Equations 6.6 and 6.7 the height error, σ_h, as a function of the phase noise is found to be

$$\sigma_h = \frac{\lambda\rho\sin(\theta)}{2\pi m B\cos(\theta-\alpha)}\sigma_\phi \tag{6.9}$$

Equations 6.8 and 6.9 allow the generation of an error map showing the local height accuracy for each post in an interferometrically derived DEM.

Typically, the post spacing of the IFSAR topographic data are comparable to the fine spatial resolution of SAR imagery while the altitude measurement accuracy generally exceeds stereoscopic accuracy at comparable resolutions. The registration of the two SAR images for the interferometric measurement, the retrieval of the interferometric phase difference and subsequent conversion of the results into digital elevation models of the terrain can be highly automated, representing an intrinsic advantage of the IFSAR approach. The performance of IFSAR systems is largely understood both theoretically and experimentally enabling these system to be designed and built to meet specific mapping objectives. These developments have led to airborne and spaceborne IFSAR systems for routine topographic mapping.

---

[4] The Cramer Rao bound used to relate the phase noise to correlation and number of looks is only valid when the number of looks exceeds 4 or 5. The number of looks in most interferometric systems used to generate topographic maps usually is much larger than 4. A notable exception is the SRTM system (described later in the chapter) where the number of looks varied between 1 and 4.

For the remainder of this chapter IFSAR is defined as an airborne or spaceborne interferometric radar system, flown aboard rotary or fixed wing aircraft, or any space based platform, that is used to acquire 3-dimensional coordinates (these coordinates must be convertible to a specified geographic datum) of terrain and terrain features that are both manmade and naturally occurring. IFSAR systems consist of a platform, GPS and attendant GPS base station(s) if needed, INU and interferometric radar system including commanding and data acquisition systems. The system may also include other ancillary equipment such as baseline metrology systems as necessary for accurate map generation. These systems form synthetic aperture images of terrain surfaces from two spatially separated antennas over an imaged swath that may be located to the left, right or both sides of the imaging platform.

DEVELOPMENTAL HISTORY

Radar interferometry has a relatively short history, with the first instances occurring in the late 1960's for planetary radar observations. Rogers and Ingalls [Rogers and Ingalls, 1969] reported using interferometry to remove the "north-south" ambiguity in range/range rate maps of the planet Venus from Earth-based antennas. Later, Zisk [Zisk, 1972] applied a similar methodology to measure the topography of the Moon.

Radar interferometry for Earth based topography measurement had its genesis with an airborne SAR system by Graham in the early 1970's [Graham, 1974]. Graham modified the system with an additional physical antenna displaced in the cross-track plane from the original SAR antenna to form an imaging interferometer. By mixing the signals from the two antennas in hardware, the Graham interferometer recorded amplitude variations that represented the relative phase of the signals. As discussed above these relative phase changes are sensitive to the topography of the surface and thus the resulting fringe patterns tracked the topographic contours.

The rapid advance in digital processing techniques and hardware in the late 1970's and early 1980's enabled subsequent IFSAR systems to record and process the complex amplitude and phase information digitally for each antenna. This obviated the need for combining the signals in hardware as done in the Graham interferometer, thereby overcoming the difficulty of trying to invert the amplitude fringes for quantitative topography measurements. Demonstrations of the first airborne [Zebker and Goldstein, 1986] and spaceborne [Li and Goldstein ,1990] interferometric systems employing this technique were conducted by researchers at the Jet Propulsion Laboratory in the late 1980's.

Rigorous assessment of SAR interferometry for topography mapping was first done using the NASA/JPL TOPSAR interferometric radar system [Madsen et al, 1993]. TOPSAR, an extension of the multi-purpose JPL AIRSAR radar system that features fully polarimetric C-, L- and P-band frequency radars, originally consisted of a C-band (5.6 cm wavelength) interferometer [Zebker et al, 1992]. It was later augmented with an L-band (24 cm wavelength) interferometer. The TOPSAR system uses two C-band antennas that are flush mounted on the left side of the JPL/NASA DC-8 aircraft as shown in Figure 6.18. With an approximately 12 km swath and 2-3 m height accuracy at 5 m postings, TOPSAR proved (and continues to prove) a valuable testbed for understanding the capabilities and limitations of interferometric radar systems.

Although the first demonstrations of spaceborne interferometric SAR used the L-band SAR aboard the SEASAT satellite and the Magellan S-band SAR that mapped the surface of Venus, it was the launch of the European ERS-1 (1991) and ERS-2 (1995) satellites that spawned international interest in interferometric SAR research. ERS satellites collect interferometric data in the so-called repeat pass mode where data is collected on two nearly identical flight tracks separated in time. Repeat pass observations can be used to generate topographic maps and surface deformation maps [Zebker et al, 1994]. Topographic maps generated from repeat pass observations have two additional error sources resulting from changes between observation times. See below for a more detailed discussion of repeat pass interferometry. The first error source is due to changes in

Figure 6.18 View of the NASA DC-8 in flight with the AIRSAR and TOPSAR antennas clearly visible where they are mounted on the fuselage. See color plate in Appendix C.

the surface (recall these only need to be on the order of a wavelength) that cause decorrelation and therefore increased height noise. The second source is due to changes in the atmosphere between observations that cause phase distortions. To demonstrate the capability of this approach on a global scale, the European Space Agency has operated the ERS-1 and ERS-2 satellites in a so-called "tandem mission" approach. The two spacecraft obtained SAR measurements for a significant fraction of the earth's surface with measurements from one spacecraft one day after those from the other, with the two spacecraft in nearly the same orbital configuration. The one day separation in the observations was chosen to minimize the changes in the surface and atmosphere mentioned above. Although a detailed quantitative report is not yet available, rather severe temporal decorrelation, even with a one day repeat observation interval, has been observed especially in heavily vegetated areas. When a detailed quantitative report from this large data set becomes available, it will be an important resource for DEM users and future IFSAR mission designers to assess the potential accuracy of such products.

In the early 1990's, based on the success of TOPSAR and other results, the Defense Advanced Research Projects Agency (DARPA) saw the potential for radar interferometric mapping systems to meet a variety of military and civilian needs. Under DARPA sponsorship the IFSARE radar system [Sos et al, 1994], designed and built by ERIM with system engineering support and an interferometric processor supplied by JPL, was the first system specifically engineered to meet a set of topographic mapping requirements. A key system requirement for IFSARE was to map absolute elevations, without the need for ground control, to meter level accuracy. Flown on a LearJet36 with operational altitudes up to 10,000 m, IFSARE uses a combination of differential GPS (DGPS) and a state of the art INU to obtain accurate position and attitude information. To insure baseline stability as a function of temperature, the interferometric antennas are mounted on an Invar frame attached to the bottom of the aircraft. A series of rigorous tests designed to evaluate system performance versus engineering predictions showed the system met or exceeded all mapping requirements. Subsequently, the IFSARE system, renamed to STAR-3i and operated by Intermap, became the first commercially operational interferometric mapping radar.

In 1994 NASA twice flew the third in a series of Space Imaging Radars (SIR-C) in partnership with the Italian and German Space agencies. SIR-C/X-SAR was fully polarimetric at C- and L-bands and operated in the vertically polarized state at X-band. For the last three days of the second mission, the shuttle position was controlled to have nearly exact repeat orbits separated by 1 day. Some of the data collections in the second mission were designed for repeat pass observations over sites collected during the first mission six months earlier. Interferometric studies from SIR-C/X-SAR contributed to a further understanding of the relative temporal decorrelation rates at X-, C-, and L-bands, increased the understanding of atmospheric propagation effects, and provided the first insights into how polarization affects interferometric phase.

Chapter 6   159

The two very successful flights and the high quality interferometric products generated during the mission led to a dedicated interferometry space mission. This mission, the Shuttle Radar Topography Mission (SRTM) has finally achieved a 3 decades long elusive goal of obtaining a highly accurate globally consistent topographic map of the Earth's surface [Farr and Kobrick 2001].

The National Aeronautics and Space Administration (NASA) in conjunction with the National Imagery and Mapping Agency (NIMA) – now the National Geospatial-Intelligence Agency (NGA) of the US – developed SRTM to address some of the limitations of repeat pass interferometry discovered by ERS and SIR-C/X-SAR. The SIR-C/X-SAR radar was augmented with radar antennas mounted on a 60 m deployable boom. Radar interferometric data was collected at C- (5.6 cm wavelength) and X- (3 cm wavelength) bands. The SRTM C-band radar system collected data for 99.97% of the Earth's landmass between –57° and 60° latitude during an 11 day mission in February, 2000. By combining the data from both ascending and descending orbits a seamless mosaic of the Earth's topography was generated. The topography data have an absolute height measurement accuracy (90% confidence level) of about 9 meters with a post spacing of about 30 m. This is the first synoptic measurement of the Earth's topography processed in a globally consistent fashion. Data from SRTM at a 90 m posting is freely available for download for all areas mapped worldwide and at 30 m posting for the US and its territories. It has already had many scientific, civilian and military applications.

Continued proliferation of interferometric SAR systems for topography and other applications is a testament to the success of the technology. Today there are over a dozen airborne interferometers operated by governments, universities and commercial organizations. There have been a large number of spaceborne SAR instruments flown in recent decades: ERS-1 and ERS-2 satellites operated by the European Space Agency, JERS-1 operated by the National Space Development Agency of Japan, RadarSAT-1 operated by the Canadian Space Agency, and SIR-C/X-SAR operated by the United States, German, and Italian space agencies. Planned spaceborne SAR instruments such as ENVISAT by the European Space Agency, ALOS PALSAR by National Space Development Agency of Japan, and RadarSAT-2 by the Canadian Space Agency will continue to spawn new technology and applications.

TYPES OF SENSORS

Interferometric SAR systems come in a variety of configurations and operate over a diverse set of frequency, resolution and accuracy regimes. Here we outline elements common to all interferometric mapping systems and describe some of the tradeoffs between the various configurations. This treatment is geared for DEM users who need to understand how best to select a system that accommodates their mapping requirements.

Categorizing IFSAR systems by the platform type, airborne or spaceborne, and method of data collection, single-pass (SPI) or repeat-pass (RPI), yields four major implementations with various relative strengths and weaknesses. Regardless of implementation these systems have a number of elements in common. Constructing accurate height maps using radar interferometry requires precise knowledge of the platform position, attitude, and interferometric baseline as well as knowledge of the radar operating parameters. Phase stability and tracking of any phase changes not a result of topographic variations are also key considerations for IFSAR mapping systems.

Interferometric observations are made with both antennas on the same platform[5], referred to as single-pass interferometry (SPI), or from multiple observations separated in time, referred to as repeat-pass interferometry (RPI) as illustrated in Figure 6.19. Repeat pass observations may be separated by as little as a fraction of a second or may be many years apart. RPI is possible when

---

[5] In principal the antennas could be on separate platforms flying in formation. Several global IFSAR mapping missions have been proposed using formation flying satellites to achieve the required baseline lengths, however to date none has flown [Zebker et al, 1994].

the flight tracks are separated by less than the critical baseline length and when the surface has not changed enough to cause decorrelation. Atmospheric changes between observations, particularly those attributed to tropospheric water vapor, can dramatically alter interferometric phase measurements [Goldstein, 1995], [Zebker et al, 1997] and [Tarayre and Massonnet, 1996]. Spatial scales for atmospheric phase distortion effects are typically on the order of kilometers and scale indirect proportion to wavelength. The effect on interferometric height measurements can be a meter to hundreds of meters depending on the amount of distortion and the baseline length. Spaceborne SARs flying above the ionosphere (orbits above 300 km) also experience phase distortions due to changes in the ionosphere between repeat observations, however these changes typically have larger spatial scales of 10-100 kilometers and have a non-linear wavelength dependency. The non-linear wavelength dependence offers the possibility of removing ionospheric distortion by flying a multi-frequency system, similar to the way GPS corrects for the ionosphere using two frequencies.
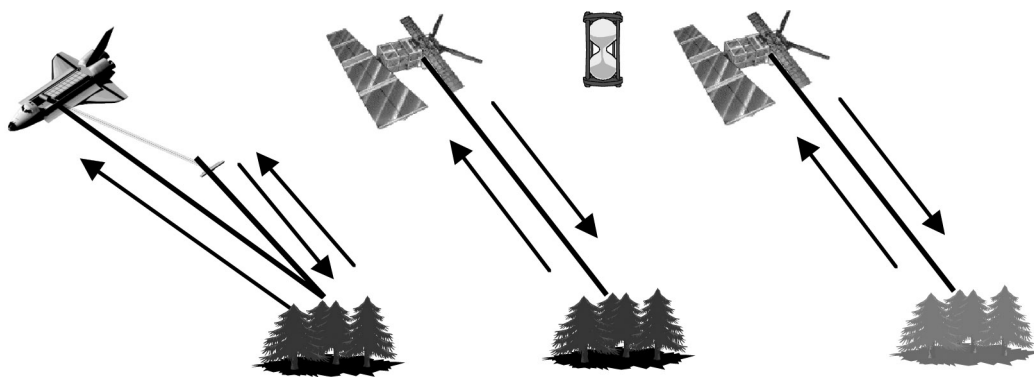
Figure 6.19 Interferometric radar topographic measurements are made with single pass and repeat pass systems. With single pass systems two spatially separated antennas (usually on the same platform) are arranged to collect echoes from the terrain simultaneously. The left side of the figure shows the SRTM mapping radar, which had two antennas separated by a 60 m retractable boom and made interferometric radar observations for much of the Earth's surface. With repeat pass systems the scene is imaged at least twice separated by an interval of time that may be seconds to years. The right side of the image shows the ERS radar satellite imaging the same area twice. The time interval for repeat pass ERS observations were as short as 1 day during the tandem phase of operation and have spanned many years.

Surface change between observations has two effects on the interferometric measurement. The first, discussed previously, is loss of correlation when change occurs within a resolution element. These changes need only be a fraction of a wavelength, such as vegetation blowing in the wind or snow falling, to cause decorrelation severe enough to make topographic mapping impossible. Secondly, the surface can deform in a systematic manner such that the elemental scatterers within a resolution element remain largely unaltered. Examples of this include inflation from volcanoes, earthquake displacement, subsidence due to water or oil pumping, and glacier motion. In contrast to topography where the amount of phase change depends on the length of the baseline, phase distortions due to surface motion are independent of baseline. The direct coupling of surface motion interferometric phase measurement to the range rather than the baseline results in a much greater sensitivity of the interferometric phase to surface motion than to topographic variability. Placing this in perspective, for a typical IFSAR configuration the sensitivity of phase to topography is roughly a change of 2π radians for a hundred meters of relief, whereas the phase changes by 2π radians from surface motion of centimeters[6]. For RPI

---

[6] More precisely, surface motion of half a wavelength results in a change of 2π in the interferometric phase.

topographic mapping applications, it is essential to avoid areas where there has been surface motion between observations as this results in major distortions to the topographic map. However, with proper processing techniques it is possible to exploit the sensitivity of IFSAR observations to surface motion to measure millimeter level surface deformation of very wide areas. These observations have become an essential part of the investigations of many solid earth scientists studying earthquakes, volcanoes, and glaciers. The possibility of using these observations for making topographic map corrections is discussed later in the chapter.

Position, Attitude and Baseline Metrology

Position measurement with the advent of GPS and DGPS systems and very good INSs enables very accurate motion measurement on a broad range of time scales. Kinematic GPS used with either airborne or spaceborne platforms achieves decimeter absolute position accuracy with a 2 Hz sampling rate. Although 2 Hz sampling of the motion works for satellites that have relatively smooth trajectories, faster sampling of 20 Hz or greater is required for airborne IFSAR applications. INU systems provide the faster motion and attitude update rates needed for motion compensation. Blending of kinematic DGPS and INU data is an increasingly common method of optimizing position and attitude data to have a high effective sampling rate and excellent absolute position accuracy necessary for airborne applications..

For interferometric applications it is knowledge of the antenna locations that is essential and required for baseline determination and motion compensation. Rarely are the motion metrology systems mounted to the center of the antenna, therefore platform attitude measurements coupled with measurements of the antenna location relative to the motion sensors is needed. Absolute angle determination with accuracy of approximately a few thousandths of a degree is off-the-shelf technology today with tightly coupled INS/GPS systems, significantly improving the critical determination of the baseline orientation angle. For spaceborne platforms, star trackers provide absolute attitude measurements with 1-10 arcsecond accuracy. If faster update rates are needed then star tracker measurements are coupled with IMU measurements.

It is not always possible to design IFSAR systems such that the antennas remain fixed relative to the motion measurement system. When this is the case additional metrology devices are required to track antenna motion with respect to the platform. Very few systems thus far have been fitted with active baseline metrology systems but those that have used a combination of optical ranging and target tracking devices. Update rates for these systems are matched to the expected motion of the antenna relative to the platform to insure proper baseline determination.

Spaceborne radars, until recently, have relied upon Doppler tracking for orbit determination. Doppler tracking can determine satellite positions with accuracy from 10 cm to 100 m depending on the orbit and the amount of tracking data available. The highest accuracy Doppler derived orbit position data may fall short of the accuracy requirements needed for RPI topographic mapping. Baselines that must be known to a centimeter or even sub-centimeter accuracy cannot be determined strictly using Doppler tracking data. Ground truth in the form of existing DEMs or radar identifiable ground control points are used to determine the baseline for RPI topographic applications when adequate metrology is not available.

Frequency Selection

Frequency selection is often a trade among scientific considerations, technology readiness, platform constraints, frequency availability and cost. Ideally, the choice of frequency would be tailored to electromagnetic properties of the surface of interest. However, the varied nature of the Earth's terrain precludes any single frequency from satisfying all possible application requirements. For example, higher frequency systems interact with the leafy crowns and smaller branches so the interferometric height more closely follows the top of the vegetation canopy. Lower frequencies penetrate deeper into the canopy and interact more with the larger branches and ground-trunk junctures so the measured height more closely follows the ground surface. One

estimate or the other may be more desirable depending on the application. For RPI topographic systems, lower frequency systems are usually preferred since temporal decorrelation is less than for higher frequency systems, particularly in vegetated regions.

Practical considerations may also be important, especially when there are platform constraints on weight, power or volume. For a given baseline length the higher the frequency the greater the sensitivity to topographic variation. Therefore, for a platform where the baseline length is fixed, one way to increase the mapping accuracy is to increase the frequency. Antenna size is inversely proportional to the wavelength so lower frequency systems generally need larger antennas. Propagation differences for different frequencies can also affect selection. Spaceborne radars flying above the ionosphere experience greater phase propagation distortion as the frequency decreases. Both international and national organizations regulate frequency spectrum usage that further restricts selection. In particular, mapping systems that require a wide bandwidth for fine resolution mapping may have more difficulty in certain bands.

Airborne-Single Pass

Single pass aircraft systems are well suited for generating fine resolution regional scale DEMs. An example of regional mapping using TOPSAR, an airborne IFSAR system, is shown at Figure 6.20. Aircraft systems have a great deal of flexibility in scheduling data acquisitions, orientation of flight lines, and modes of operation. Single pass systems are best suited for generating high quality topographic maps to a specified absolute accuracy since they do not suffer from temporal decorrelation or from atmospheric phase distortion problems.


Figure 6.20 Radar DEM of the Napa Valley. This view of Napa Valley, California and the surrounding area was created with data from NASA's Airborne Synthetic Aperture Radar while it was being flown in its topographic (TOPSAR) mode on a NASA DC-8 aircraft. The colors in the image represent topography, with blue areas representing the lowest elevations and white areas, the highest. Total relief in the image is approximately 1400 meters. The height information has been superimposed on a radar image of the area, which was collected simultaneously. The image is 70 by 90 kilometers with the Napa Valley the broad flat long area (green—blue) in the center left of the image. Lake Berryessa is the dark area in the center right of the image. See color plate in Appendix C.
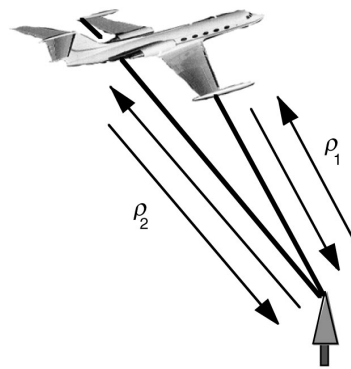
Two modes of aircraft interferometric data collection are common; single antenna transmit (SAT) mode where one antenna transmits and both receive and Ping-Pong mode where each antenna transmits and receives its own echoes as shown in Figure 6.21.

Single Antenna Transmit
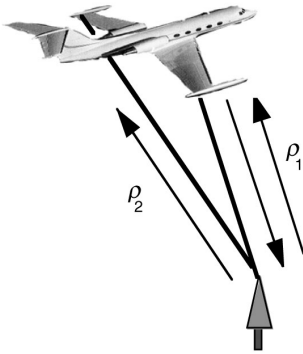
Ping-Pong

Transmission from one antenna
Reception through both antennas simultaneously

Alternately transmitting out of two antennas
Reception through the same antenna used for
transmission only

Figure 6.21 Illustration showing the two means of data collection used on SPI IFSAR systems. In Single Antenna Transmit mode (SAT) a pulse is transmitted from one antenna and the echo recorded from two receiving antennas whereas for Ping-Pong systems each antenna separately transmits and receives.

In SAT mode, the total phase difference is

$$\delta\phi = \frac{2\pi}{\lambda}\{\rho_1 + \rho_1 - (\rho_1 + \rho_2)\} = \frac{2\pi}{\lambda}\{\rho_1 - \rho_2\} \qquad (6.10)$$

where ρ_i is the range from antenna A_i to a point on the surface. In Ping-Pong mode, the interferometric phase is given by

$$\delta\phi = \frac{2\pi}{\lambda}\{\rho_1 + \rho_1 - (\rho_2 + \rho_2)\} = \frac{4\pi}{\lambda}\{\rho_1 - \rho_2\} \qquad (6.11)$$

Equations 6.10 and 6.11 show that the interferometric phase in Ping-Pong mode is twice that of SAT mode, such that Ping-Pong operation effectively implements an interferometric baseline that is twice the physical baseline. The advantage of operating in Ping-Pong mode is the larger effective baseline increases the interferometric height acuity by a factor of two compared with SAT mode. However, the increased baseline length causes the phase to change faster and in steep terrain can lead to areas that cannot be unwrapped. For those systems that have a choice of operating in either mode, the selection depends on the amount of topographic relief.

Airborne-Repeat Pass

Airborne repeat pass IFSAR systems for topographic mapping enjoy the same operational flexibility as SPI IFSAR systems, namely, scheduling of data acquisitions, orientation of flight lines, and modes of operation [Gray and Farris-Manning, 1993]. In principle, repeat pass systems

have increased baseline flexibility because repeat tracks could be flown having any desired baseline length and orientation. Intelligently matching the baseline length to the terrain, or by combining multiple data sets with varying baselines, opens the possibility of generating topographic products with increased accuracy. In practice, controlling the repeat flight pass geometry with precision is extremely difficult. Typically, useful baseline lengths are in the range of 10-100 meters and, to avoid variable quality problems, should remain parallel. Standard flight management systems do not support such accuracy. Several IFSAR mapping systems have been modified to support repeat pass interferometry, including the Danish EMISAR system [Madsen et al, 1996], which is operated on a Royal Danish Air Force Gulfstream G-3 and Aerosensing's Turbine Commander aircraft. The EMISAR system has demonstrated a track repeatability of 10 m which is sufficient for many applications but certainly falls short of being able to fly with any desired baseline.

Although repeat pass systems have increased baseline flexibility they suffer from several problems not present in SPI system. Temporal decorrelation in foliated areas and changes in the terrain even for very short time intervals can be severe. Figure 6.22 shows airborne repeat pass interferometric data at C-, L-, and P-bands acquired using the NASA/JPL AIRSAR system [Hensley et al, 1995]. Although the flight tracks were only separated by 20 minutes, the windy conditions caused decorrelation at all three frequencies. The amount of decorrelation increases as the wavelength decreases. Atmospheric changes between passes can cause phase distortions that lead to height errors that are difficult to detect and remove.
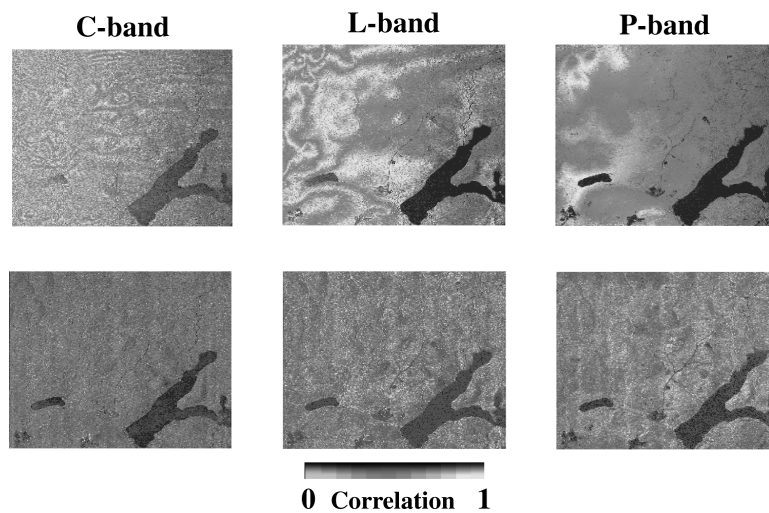
C-band **L-band** **P-band**

0 Correlation 1

Figure 6.22 Airborne repeat pass interferometric observations at Portage Lake, Maine made with the AIRSAR system. The top row shows the interferometric phases for C-, L- and P-bands. At bottom are the corresponding correlation maps. Conditions were windy when the data was collected and the branch movement resulted in greater decorrelation at shorter wavelengths. See color plate in Appendix C.

To generate accurate topographic maps using RPI IFSAR systems, the baseline must be accurately determined. Kinematic DGPS solutions for aircraft motion have an accuracy of 2-3 cm. Typical interferometric baseline accuracy requirements are at the millimeter level, an order of magnitude finer than the capability of current metrology. Determining the baseline at this level of accuracy must be done using the data and some form of ground control. Aircraft motion, unlike spacecraft motion, is not very smooth and solving for airborne RPI baselines is quite difficult. Because of this it has thus far proven very difficult to calibrate these systems for absolute accuracy.

Spaceborne-Single Pass

Spaceborne platforms have the advantage of global and rapid coverage and accessibility. Increased coverage for spaceborne systems comes about from the combination of the faster velocity by a factor of 30 and the larger swath widths ranging from 50-500 km. Spaceborne systems also avoid airspace restrictions that make aircraft operations difficult in certain parts of the world. Typical baselines for spaceborne IFSAR system making topography measurements range from 100-1000 meters. Baseline accuracy requirements are similar to airborne platforms, requiring millimeter length and arcsecond orientation angles knowledge. This poses a difficult metrology problem regardless of whether the antennas are connected to the same platform or are on separate platforms flying in formation. Tracking phase instability of the radar hardware and antennas, which may go through a hundred degrees Celsius or more of temperature change in an orbital period, requires special hardware. SRTM is the only spaceborne SPI IFSAR system to have flown thus far and will be described in greater detail later.

Recently approved is the Tandem-X mission whereby the German space agency, DLR, in partnership with EADS Astrium GmbH and InfoTerra GmbH, plans to fly two nearly identical X-band SAR systems with tightly controlled orbits with the goal of producing global DTED-3 (12 m posting with better than 2 m height accuracy) for the world. The system has numerous other modes and capabilities (e.g. ocean current and traffic velocity mapping) that will tested after is planned launch in 2009. Of particular interest to the topographic mapping community is that Tandem-X system is fully polarimetric offering the possibility to estimate the vegetation bias (at least for some vegetation types) using the recently developed techniques of polarimetric radar interferometry. Topographic data generated by Tandem-X will be available commercially through the industrial partners of DLR. Tandem-X is posed to be the successor to SRTM and provide the next generation higher resolution and accuracy global DEM of the Earth.

Spaceborne-Repeat Pass

Repeat pass interferometric observations have their greatest utility in measuring surface deformation over wide areas for geophysical applications such as earthquake monitoring, volcano inflation and deflation, and glacier motion. Nonetheless, RPI IFSAR has been used to make topographic maps in many parts of the world, often exceeding the accuracy of the best topographic maps currently available in those regions. Figure 6.23 shows a map of Ft. Irwin, CA made with repeat pass SIR-C. Comparison with a TOPSAR mosaic of the same area showed the height accuracy of $RMSE_z = 16$ m. The height difference map in Figure 6.23 shows tropospheric water vapor induced error that in this case was the dominant error source. If DEMs from multiple independent pairs of repeat pass observations are available, these can be averaged to reduce both atmospheric and random noise.
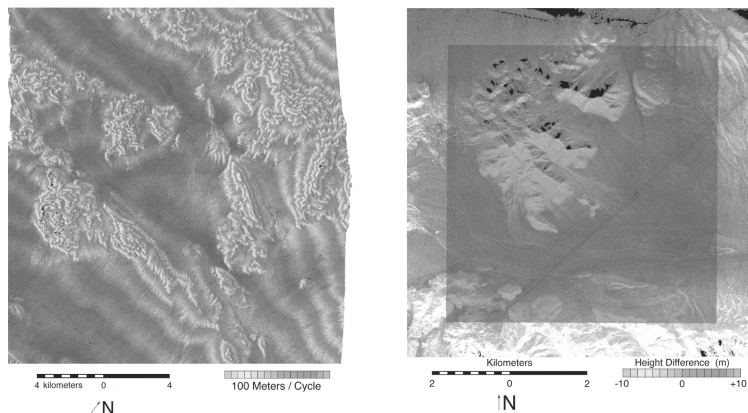

Figure 6.23 IFSAR DEM of Ft. Irwin, CA generated using SIR-C C-band one day repeat pass data collected during the October, 1994 flight of the instrument. The limiting source of error is most likely a result of changes in tropospheric water vapor between passes. See color plate in Appendix C.

Besides tropospheric or ionospheric propagation effects to the interferometric phase as seen in the last example, the other major limiting factor to RPI IFSAR topographic map generation is temporal decorrelation. Figure 6.24 shows decorrelation on the island of Hawaii, for one, two and three day repeat observations, using C-band and L-band data acquired during the second SIR-C mission. Similar to the aircraft RPI example shown earlier, the lower frequency L-band is better correlated than the C-band data for all repeat intervals. The unpredictability of the amount of decorrelation, (in this case the 3 day repeat interval had greater correlation than the two day repeat interval), complicates the process for obtaining suitable repeat pass pairs.

Table 6.3 summarizes the discussion of the various types of IFSAR systems.
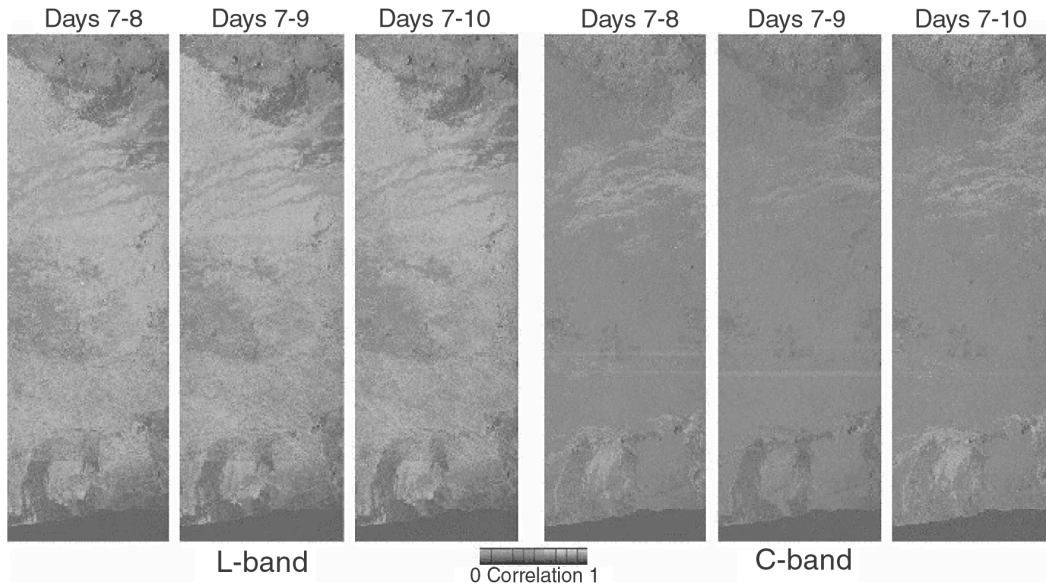
Figure 6.24 Correlation maps produced for one, two and three day repeat pass intervals at C-band and L-band obtained during the second SIR-C mission. See color plate in Appendix C.

Table 6.3 Summary of Types of IFSAR Systems.

	Single Pass	Repeat Pass
Airborne	Regional Coverage Affordable Fine Resolution Necessary Motion Compensation Benign Atmospheric Effects No Temporal Decorrelation No Ionospheric Effects Possible Need for Active Baseline Metrology	Regional Coverage Affordable Fine Resolution Necessary Motion Compensation Problematic Atmospheric Effects Temporal Decorrelation Effects No Ionospheric Effects Difficult Track Repeatability Difficult Baseline Estimation Change Detection Possible Increased Baseline Flexibility
Spaceborne	Global Coverage Costly Fine Resolution Benign Motion Compensation Benign Atmospheric Effects No Temporal DecorrelationProblematic Ionospheric Effects Baseline Metrology Required	Regional Coverage Costly Fine Resolution Benign Motion Compensation Problematic Atmospheric Effects Temporal Decorrelation Effects Problematic Ionospheric Effects Difficult Track Repeatability Benign Baseline Estimation Change Detection Possible

PRESENT OPERATING STATUS

With widespread availability of spaceborne radar data acquired in the 1980's by ERS and RadarSAT, many companies now offer RPI-based IFSAR DEMs and associated products. Several of these also sell software that allows users themselves to generate products from raw data. The quality of these products depends on the number of repeat pass pairs available over the region of interest, the amount of decorrelation and atmospheric distortion, and baseline length for the interferometric pairs. The principal companies marketing these technologies and products are Gamma, MDA, TerraSAR and Vexcel. However, the most accurate and reliable sources of IFSAR DEM data are generated using SPI systems. The remainder of this chapter, with one exception, is devoted to brief descriptions of currently commercially operational or soon to be commercially operational SPI IFSAR systems. These systems are airborne systems designed for commercial operational mapping and are operated by Intermap Technologies Inc. and EarthData International. SRTM is the exception since DEMs generated from this government mission are appearing in many commercial and civilian applications.

Intermap Technologies / STAR Systems[7]

Intermap Technologies Inc. currently operates three airborne IFSAR systems with two additional systems under development that will be in operation by late 2006. Intermap's first IFSAR system, STAR-3i®, has been operated by Intermap since 1996. It was initially developed by ERIM (Environmental Research Institute of Michigan) and referred to as IFSARE in the early literature. STAR-3i is an X-band, HH polarization IFSAR flown on a Learjet 36 [Tennant and Coyne, 1999]. In the last few years, Intermap has replaced all of the software and most of the hardware in order to improve product quality and efficiency of operation. In particular this has led to higher resolution images, and better vertical accuracy of the DEMs. Equally important, software automation has led to improvements in processing throughput. The net result of the modifications is higher quality data sets moving toward decreasing costs and wider availability.

Intermap's second system is named TopoSAR® (formerly called AeS-1). It is one of several systems developed by AeroSensing GmbH [Schwäbisch and Moreira, 1999], still operated by Intermap and is currently flown on an Aerocommander turbo-prop platform. In addition to X-Band, HH single-pass IFSAR, it supports repeat-pass, fully polarized P-Band IFSAR. Intermap modified this system in 2005 to allow simultaneous acquisition of the X-Band and P-Band channels. While the system design philosophy originally was quite different from that of the STAR-3i system, the processing stages and the specifications of the X-Band products are now identical. This commonality is achieved via the STAR-4 architecture, technology developed by Intermap in 2003 incorporating the best of the preceding architectures. The STAR-4 architecture was designed to provide the improved products and increased capacity needed to satisfy Intermap's NEXTMap nation wide acquisition programs. Intermap's third system is based completely on the new STAR-4 architecture and is flown in a King Air prop-jet. Two new systems based on the STAR-4 architecture are under construction in 2006 and will be flown in Lear Jet and KingAir platforms and will be named STAR-4 Lear2 and STAR-4 KA2. Current specifications of all five systems are summarized in Table 6.4. Plans are also in place to upgrade STAR-3i to the STAR-4 architecture.

To ensure the final product is precise, accurate and consistent, all Intermap systems utilize a stable fixed baseline on which the antennae and inertial measuring device are co-located. This fixed baseline is critical to accuracy as 1-mm of error in baseline length translates to several meters of elevation error. Co-location of the IMU improves accuracy as it allows accurate measurement of the baseline position and orientation; small errors in these parameters lead to large errors in the elevation solution. All Intermap systems use a single transmit/receive chain which provides double the effective baseline as the interferometer operates in ping/pong mode. A single chain also minimizes calibration errors as all signals travel the same system paths. The motion data and

---

[7] This section was provided by Intermap to describe the operating status of their IFSAR systems.

auxiliary radar data are stored on the control computer for subsequent processing. All sensor positioning is managed using post processing DGPS/INS processing SW that was developed by Intermap. There is no radar processing on board; radar signal data are recorded directly to an onboard disc system capable of storing over 1 Terabyte which is sufficient to acquire 4 – 5 lines, 450km in length, in one flight. Data are transcribed to LTO-3 data tapes in the field and are transferred to the processing center for generation of the final products.

Table 6.4 System Parameters of Intermap IFSAR.

Parameter	STAR-3i	STAR-4 KA1	STAR-4 Lear2	STAR-4 KA2	TopoSAR X-Band	TopoSAR P-Band
Operational year (Initial)	2002 (1996)	2004	2006	2006	2005 (1996)	2005 (2000)
Platform	Lear 36	King Air 200T	Lear 36	King Air 200T	Aero Commander 685	Aero Commander 685
Wavelength	3 cm	3 cm	3 cm	3 cm	3 cm	74 cm
Peak Transmit Power	8 kW	8 kW	8 kW	8 kW	2.5 kW	1.1 kW
Center Frequency	9.605 GHz	9.605 / 9.675 GHz	9.605 / 9.675 GHz	9.605 / 9.675 GHz	9.605 GHz	375 MHz
Bandwidth	135 MHz	135 / 270 MHz	135 / 270 Mhz	135 / 270 MHz	135 MHz	67 MHz
Antenna Beam Width	1.45°	3.95°	1.45°	3.95°	8.1°	33°
Baseline Length	0.92 m	1.02 m	1.04 m	1.02 m	0.92 m	Typ 80 m
Polarization	HH	HH	HH	HH	HH	Quad-Pol
Baseline Tilt Angle	1.5°	1.3°	1.5°	1.3°	1.5°	---
Platform Altitude	6 – 12 km	4 – 8.5 km	6 – 12 km	4 – 8.5 km	4 – 8.5 km	4 – 8.5 km
Swath Width (km)	8 – 15 km	6 – 11 km	8 – 15 km	6 – 11 km	6 – 11 km	4 – 10 km

Figure 6.25 The three images show the STAR-3i, TopoSAR and STAR-4 platforms respectively. TopoSAR is the only system with antennas not enclosed within a radome. Figure courtesy of Intermap Technologies Inc. See color plate in Appendix C.

The process begins with data acquisition and ends with an independent review of data quality for the products created. Acquisition efforts start with the creation of a detailed flight plan using Intermap planning SW that accounts for terrain variation and accuracy requirements. From this acquisition, logistic plans are developed. Acquisition begins with site preparation; installation of GPS ground stations and, if the requirement is for Type I or II elevation accuracy, the installation of radar corner reflectors. Flight logistics and motion processing are managed via a central facility. Upon completion of data acquisition, centrally processed motion data and raw data tapes are sent to one of the two Intermap processing centers.   These processing centers are semi-automated and have the same capacity as the aircraft. The processing center utilizes 64-bit blade computation servers that generate the intermediate strip map products which are mosaiced into image tiles. Upon completion of the mosaic, a bare earth model is created using proprietary software, and all data products are finalized for delivery to the Intermap store where they are made available for licensed purchase.

Chapter 6 169

The core products include an Ortho-rectified Radar Image (ORI), a Digital Surface Model (DSM) and the bare earth Digital Terrain Model (DTM). X-band images are at 1.25-m resolution with similar horizontal accuracy. DSM and DTM are posted at 5m spacing. The elevation products are available in three standard accuracy specifications as illustrated in Table 6.5 below. It is worth noting that all four of the STAR family of sensors are able to achieve these product specifications despite the nuance of individual system design or platform specifics. Apart from these CORE specifications, other accuracies and image/DEM resolution can be supported to meet specific customer requests. Optical/radar merged products are now also becoming available. Figures 6.26 and 6.27 are visualizations of Type II products acquired during the NextMap Britain program.

Data Availability

Data can be obtained from Intermap by either of two methods: custom project or off-the -shelf. In order to make the latter approach feasible, Intermap has been developing country-wide mapping programs under the name NEXTMap. This approach is intended to address the market issues of currency, timeliness, cost and availability. To meet these market demands the approach is to provide licensed data to the users so that ultimately the acquisition/production cost is shared by multiple users.

Table 6.5 Intermap Elevation Accuracy Specifications.

Product	Measures of Vertical Accuracy			
	Specifications		Nominal	
	RMSE	95%	Mean	Standard Deviation
DSM Type I	0.5	1.0	0.3	0.3
DSM Type II	1.0	2.0	0.7	0.7
DSM Type III	3.0	6.0	2.0	2.0
DTM Type I	0.7	1.5	0.5	0.5
DTM Type II	1.0	2.0	0.7	0.7
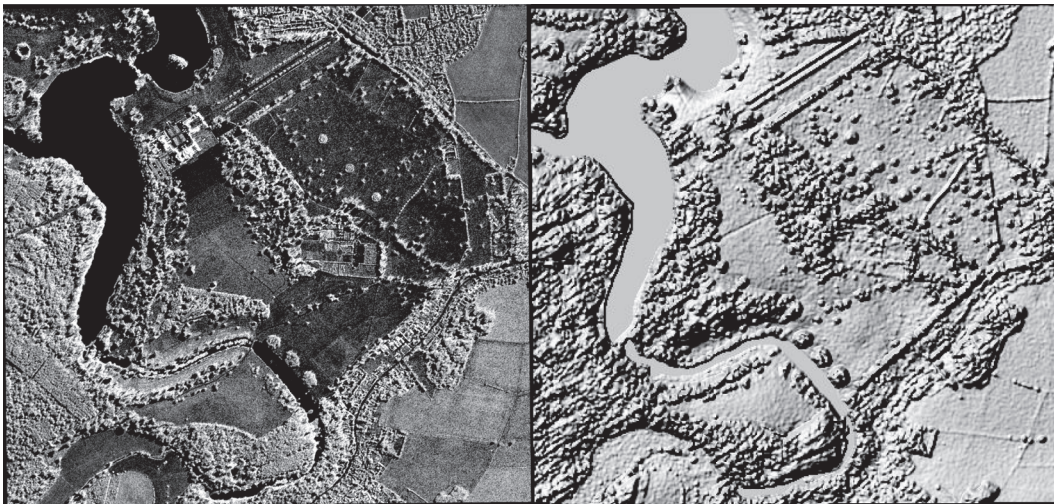
Figure 6.26 The left image is a STAR-3i ORI of Blenheim Palace, U.K. and the surrounding area while the right image is a shaded relief representation of the corresponding DSM. The images are about 2.3 km x 2.3 km. The palace is clearly defined in the upper left quadrant. Individual trees and shrubs are defined in both ORI and DSM. The texture in the open field DSM corresponds to the limiting STAR-3i elevation 'noise' - about 50 cm in this case. Figure courtesy of Intermap Technologies Inc.

Figure 6.27 The image is a three-dimensional visualization of an area in northern Wales U.K. A color air-photo has been merged with the STAR-3i DSM and presented as a perspective view or 'hill-shade'. The air-photo was supplied by GetMapping plc. Figure courtesy of Intermap Technologies Inc. See color plate in Appendix C.

TopoSAR P-band Capability

In addition to the standard X-band capabilities described above, the TopoSAR system can generate P-Band DTM products by synthesizing the interferometric baseline from two individual passes. To achieve the closer flight-line tolerance required for dual-pass interferometry, the flight management system consists of an on-line kinematic DGPS system coupled with a Honeywell LaserRef III inertial sensor. The DGPS corrections are obtained from the global OmniStar system and are downlinked to the aircraft allowing real-time 1m accuracy kinematic tracking of the flight path. This information is displayed along with the deviation relative to the desired flight track and enables the pilot to keep the position error between the actual and desired flight path to less than 10 m. The repeat-passes are usually separated in time by less than an hour, and typically at interferometric baselines of 50 to 80 meters. Tests have shown that an 80 meter baseline allows DTM extraction beneath forest canopies up to 40 meter height at the vertical accuracy level of 1.5 – 4 meter RMSE [Mercer, 2004] when working in quad-pol mode. An example of a P-Band derived DTM beneath heavy forest canopy is presented in Figure 6.28.

EarthData International/GeoSAR

GeoSAR was a program to develop a dual frequency airborne radar interferometric mapping instrument designed to meet the mapping needs of a variety of users in government and private industry. Program participants are the Jet Propulsion Laboratory (JPL), EarthData International (previously Calgis, Inc.), and the California Department of Conservation with funding provided initially by DARPA and subsequently by the National Geospatial-Intelligence Agency (NGA). Begun to address the critical mapping needs of the California Department of Conservation to map seismic and landslide hazards throughout the state, GeoSAR is currently undergoing tests of the X-band and P-band radars designed to measure the terrain elevation at the top and bottom of the
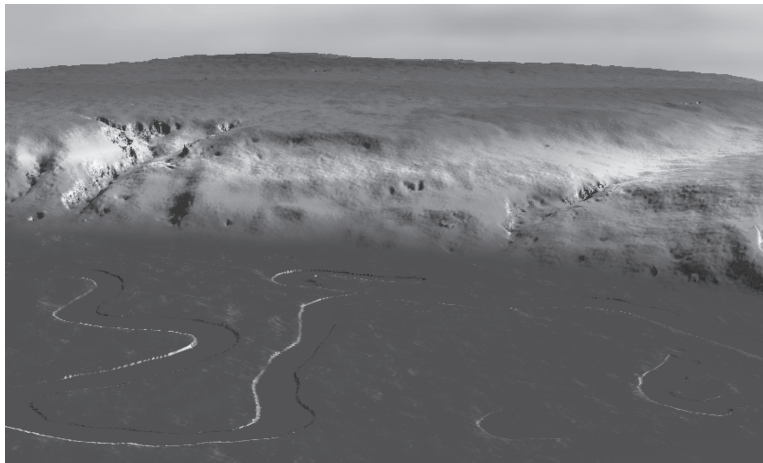
Figure 6.28 TopoSAR quad-pol P-Band DTM of test area within King County, WA, USA. The river valley was relatively bare while the steeply sloped terrain and plateau region included dense mixed forest of 10-35 meters height. Comparisons with control points and lidar 'truth' indicated RMSE differences of about 1.5-2.5m RMSE in the heavily forested plateau region but with differences growing with slope to several meters RMSE in the strongly sloped zone. Figure courtesy of Intermap Technologies Inc. See color plate in Appendix C.

vegetation canopy. Maps created with the GeoSAR data will be used to assess potential geologic/seismic hazard (such as landslides), classify land cover, map farmlands and urbanization, and manage forest harvests. This system is expected has been fully operational in 2003.

The GeoSAR radar flies onboard a Gulfstream-II aircraft and is a dual-frequency (P- and X-band) interferometric Synthetic Aperture Radar (SAR), with HH and HV (or VV and VH) polarization at P-band and VV polarization at X-band [Hensley et al, 2001]. The radar hardware onboard the Gulfstream-II aircraft is supplemented with a Laser-Baseline Measurement System (LBMS) which provides real-time measurements of the antenna baselines in a platform based coordinate system that is tied to onboard Embedded GPS/INU (EGI) Units. GeoSAR maps a 20-km swath by collecting two 10-km swaths on the right and left sides of the plane as shown in Figure 6.29.
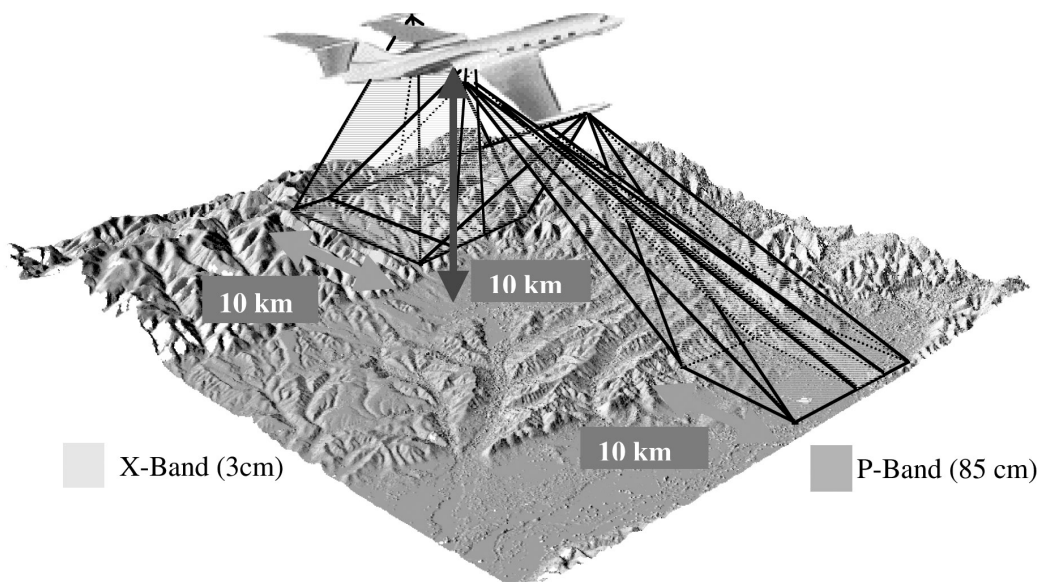
Figure 6.29 GeoSAR collects 10 km swaths simultaneously on both left and right sides of the aircraft at both X- and P-bands. See color plate in Appendix C.

The P-band antenna system is mounted in the port and starboard wingtip pods providing a long antenna-baseline of about 20 meters. X-band antennas are mounted in pairs under the wings with an antenna-baseline of 2.5 meters. Radar operations are controlled by a command disk generated preflight by the Mission Planning Software. Real-time data collection is controlled in-flight via an Automatic Radar Controller (ARC) that sets data collection windows, performs Built-In Test (BIT's) before and after each datatake, and automatically turns the radar on and off during a data acquisition. Raw radar data is recorded on high-density digital tape recorders for subsequent, post-flight processing. The onboard data collection via the Automatic Radar Controller also records navigation data from the aircraft's GPS/INU system, the laser-based antenna-baseline measurement system, and raw signal data from X- and P-band radars. Table 6.6 gives a summary of the main system parameters.

Table 6.6 GeoSAR System Parameters

Parameter	P-Band Value	X-Band Value
Peak Transmit Power	4 kW	8 kW
Bandwidth	80/160 MHz	80/160 MHz
Center Frequency	350 MHz	9.755 GHz
Baseline Length	20 m and 40 m	2.6 m or 5.2 m
Baseline Tilt Angle	0°	0°
Platform Altitude	5,000 m to 10,000 m	5,000 m to 10,000 m

Processing of the data is done on a cluster of Origin computer systems equipped with hundreds of processors and hundreds of Gbytes of RAM. The processor incorporates a number of new algorithms used to remove radio frequency interference (RFI) at P-band, focus the P-band data with its large synthetic aperture and for regridding and mosaicking the data. The expected map accuracy of the X-band system is sub-meter in bare surface regions and 1-4 m in vegetated areas through a combination of X-band and P-band data. Figure 6.30 shows height maps generated using the X-band and P-band radars over Monarch Grove, CA. The eucalyptus tree stand highlighted in the imagery shows up extremely well at X-band but is nearly undetectable in the P-band data because of the increased penetration into the canopy.
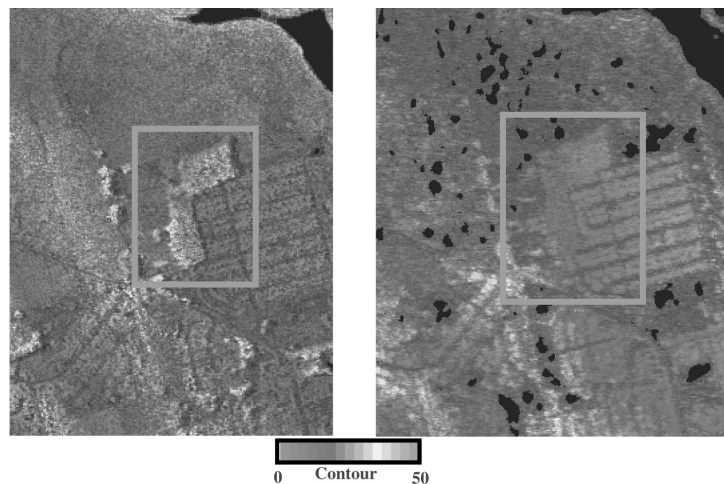

Figure 6.30 GeoSAR X-band (left) and P-band (right) DEM data collected at Monarch Grove, CA. Note the elevation contours of eucalyptus tree stand inside the orange box is clearly visible in the X-band data but barely detectable in the P-band data. The GeoSAR mapping system will use a combination of X-band and P-band data to generate bare surface elevation maps in vegetated regions. See color plate in Appendix C.

Chapter 6   173

The system has undergone a number of upgrades since in began operational service. First the system incorporated a smaller and more accurate second generation LBMS to track the interferometric baselines greatly increasing the mapping swath at X-band and reducing multi-path from the LBMS fairing leading to better calibrated products. Secondly, the system was augmented with a lidar mapping system that collects nadir pointing elevation data with 15-20 cm mapping accuracy. Lidar data are used to provide very accurate control for large area topographic mapping projects. Upgrades to the digital system replaced the high-speed tape based storage system with new disk based storage devices thereby increasing the amount of data that could be collected in a single flight line. The system is now capable of collecting data in continuous strips greater than 500 km in length. Also, upgraded at the same time were the analog-to-digital converters to provide higher fidelity radiometric and height mapping products.

NASA-NGA/SRTM

The Shuttle Radar Topography Mission system is the only spaceborne SPI IFSAR flown to date [Farr and Kobrick, 2000]. The mapping instrument consisted of modified versions of the SIR-C C-band and X-band radars that were flown on the shuttle in 1994. The most prominent modification was the 60 m retractable boom seen in Figure 6.31, with C-band and X-band receive-only antennas attached to its end. To meet the stringent mapping requirements, the SRTM mapping instrument was equipped with a specially designed motion metrology system. Absolute position information was determined from two GPS receivers located on the outboard antenna. Attitude information was derived from a combination of star tracker and IRU measurements. The interferometric baseline was measured using a combination of an optical target tracker, which measured the angles to several targets located on the outboard antenna structure, and an electronic ranging device used to measure the distance between inboard and outboard antennas. Key system and operating parameters are listed in Table 6.7.
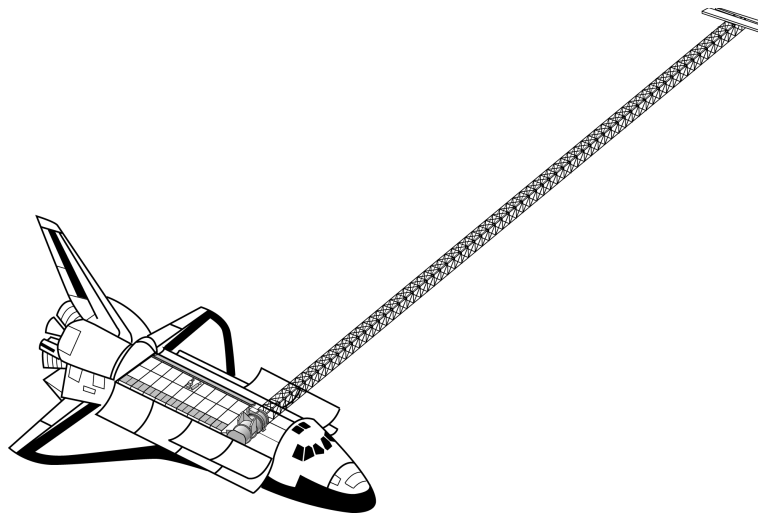

Figure 6.31 The Shuttle Radar Topography Mission (SRTM) flight system configuration. The SIR-C/X-SAR L-, C-, and X-band antennas were located in the shuttle's cargo bay. The C- and X-band radar systems were augmented by receive-only antennas deployed at the end of a 60 m long boom. Interferometric baseline length and attitude measurement devices were mounted on a plate attached to the main L-band antenna structure. During mapping operations, the shuttle was oriented so that the boom was 45 degrees from the horizontal.

Table 6.7 SRTM System Parameters

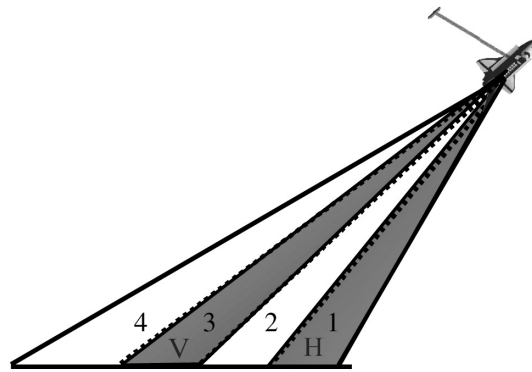| Parameter	Value
Baseline Length	62 m
Baseline Orientation Angle	45°
Wavelength	.0566 m
Burst Length	60 -100 pulses
Platform Altitude	240 km
Platform Velocity	7.5 km/s
Look Angle Range	30°-60°
Antenna Lengths	12 m/8 m
PRF Range	1330 - 1550 Hz

Figure 6.32 The SRTM C-band radar collected data in two subswaths simultaneously using horizontal (H) and vertical polarization (V). The four ScanSAR subswaths are numbered 1-4 starting from nadir as shown above.

To map the world in the 10 days allotted for the mission required the C-band radar to operate in ScanSAR mode. The C-band interferometry data was collected in swaths comprising four subswaths each as shown in Figure 6.32. ScanSAR mapping modes alternately switch between two (or more) beam positions in the cross track direction to increase the swath width at the expense of along track resolution. Exploiting the C-band polarization capability, the SRTM C-band radar operated in ScanSAR mode on vertical (V) and horizontal (H) polarizations to achieve an effective swath width of 225 km while maximizing the signal-to-noise over the swath.

Data collected onboard the shuttle was stored on approximately 300 high density tapes (approximately 6 TB of raw data). During data collection most of the mappable area was imaged two or more times from ascending and descending vantage points. Combination of these data will reduce the noise from each individual strip height map, and allow fill capability for those areas missed in a particular data acquisition (e.g. from shadow and layover). An SRTM datatake is defined as the four subswaths of ScanSAR data collected from radar collection initiation to radar collection termination. Datatake initiation usually commenced just prior to an ocean to land crossing or the start of an island group (or series of island groups) and terminated just after a crossing from land to ocean or the end of an island group (or series of island groups).

Briefly, the processing flow is as follows. Processing is done on a continent basis. All datatakes over a continent are processed from beginning to end. Each of the four subswaths of a datatake is processed independently using a specially designed ScanSAR interferometric processor. The processor generates geocoded strips of height, magnitude, correlation and height errors in coordinate system aligned with the shuttle flight direction for storage efficiency[8]. The strips then needed small adjustments to overcome small imperfections in the metrology or radar system. In conjunction with ground control points these estimates are used to adjust the data relative to the WGS-84 datum. Quality assurance measures are made after both strip map processing and mosaicking. In the event anomalies are detected, the data is queued for further analysis and potential reprocessing. Finally, the data are combined and formatted into 1° DTED 2 cells (1 arcsecond posting). Subsequent to strip map and mosaicking at the JPL the data was shipped to NGA who provided the data to two contractors who did the final data editing and brought the data set in the required DTED products specifications [Slater, et al 2006].

---

[8] Geocoding data in a sensor aligned coordinate system has other advantages. DEM errors are more easily identified and traced to their root cause when aligned with the collection geometry. Moreover, DEM mosaicking can be optimized to solve for the minimal correction parameters based on the geometry of the errors intrinsic to the sensor.
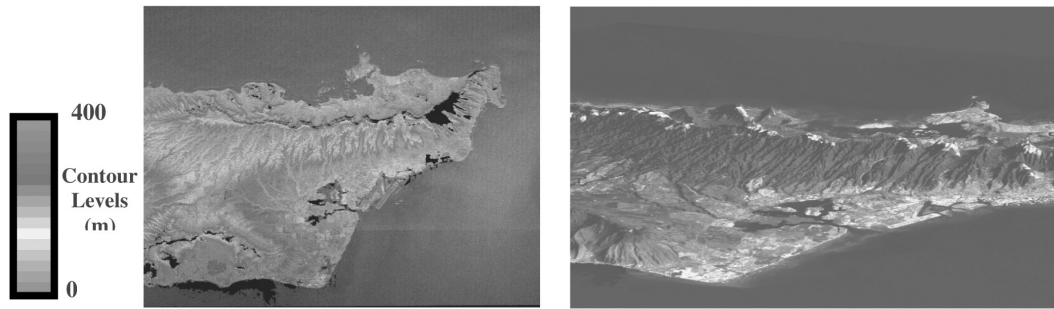
Figure 6.33 The left image of Oahu is a combination of radar backscatter with color contours overlain. Each color cycle, i.e. going from green to blue and back to green again represents 400 m of elevation change. Honolulu International Airport, Waikiki, and Diamond Head are clearly visible in the image. The right image is a perspective view using the SRTM generated topography with Landsat imagery overlaid. See color plate in Appendix C.

An example of SRTM topographic map data processed during the mission is of the island of Oahu in Hawaii. The Oahu data are from beam 2 and are posted at 30 m. These data can be combined with other sensor data shown in Figure 6.33.

An extensive validation of SRTM data has been conducted by JPL, NGA and a number of other investigators throughout the world, that showed that the SRTM data set exceeded all its accuracy specifications[9]. JPL's assessment of the SRTM data is summarized in [Rodriguez, et al, 2006] which is a condensed version of a more extensive report [Rodriguez, et al, 2005]. Analysis consisted of comparisons with continental scale kinematic GPS tracks distributed throughout the world, corner reflectors, a database of nearly 100,000 ground control points and DEM chips distributed globally. Comparison with these ground truth data sets indicated a global height accuracy of 8m (90 % confidence level) and a planimetric accuracy of better than 20m which exceeded the SRTM requirements by a factor of two. The spatial structure of the errors and the sources of these errors are described more fully in the references sited above,

All X-SAR data are the property of the German Aerospace Center DLR and the Italian Space Agency ASI. Therefore all X-SAR data except over Italy are processed, archived and distributed at full resolution by DLR. Apart from selected sensitive areas no restriction will apply. C-band raw data are owned by NGA. One arcsecond (30 m) data over the US will be publicly available, as will 3 arcsecond (90 m) data over the world. NGA will restrict access to 1 arcsecond data outside the US, however for NASA's principle scientific investigators special requests can be made to NGA via NASA. The time and method of distribution is still being decided at the time of this writing.

CALIBRATION PROCEDURES

As with any instrument designed to make quantitative measurements IFSAR systems must be properly calibrated in order to meet accuracy requirements and deliver consistent products to the user. Determining height from interferometric phase measurements requires knowledge of the platform position, range, baseline length and orientation, interferometric phase, wavelength, velocity and Doppler. Estimating systematic corrections to these parameters to obtain consistently accurate topographic maps is the essence of IFSAR calibration. First, an overview of how several key parameters effect topographic height measurement and where errors in these parameters arise is presented. This is followed by a description of the IFSAR calibration procedure.

---

[9] The March, 2006 issue of Photogrammetric Engineering and Remote sensing was devoted to papers assessing the accuracy and utility of SRTM data

Calibration Parameters

Platform Position

DGPS and INS measurement accuracy are generally the limiting factors effecting platform position errors. An error in platform position translates output position measurements in the direction of the position error. Platform position error is the only error source that is completely independent of target location. Figure 6.34 illustrates how an error in platform position translates into DEM errors.
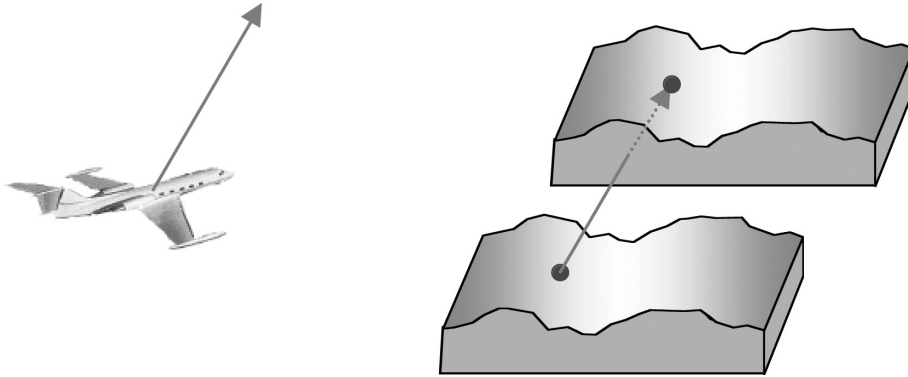

Figure 6.34 An error in platform position, indicated by the red vector in the figure, causes a translation error in the IFSAR DEM equal to the platform position error. See color plate in Appendix C.

Range

Radar range is measured by converting the time it takes for a signal to propagate from the radar antenna to the target and return to distance. Hardware timing offsets and unknown physical delays in the transmitter and receiver chains in the radar system are the major sources of range error. Range errors cause the target location to be translated along the line-of-sight vector as shown in Figure 6.35. The line-of-sight is varying across track, it moves progressively away from vertical as the cross track distance gets larger. Regardless of location within the mapping swath, horizontal and vertical distortions to the DEM are smaller in magnitude than the size of the range error.
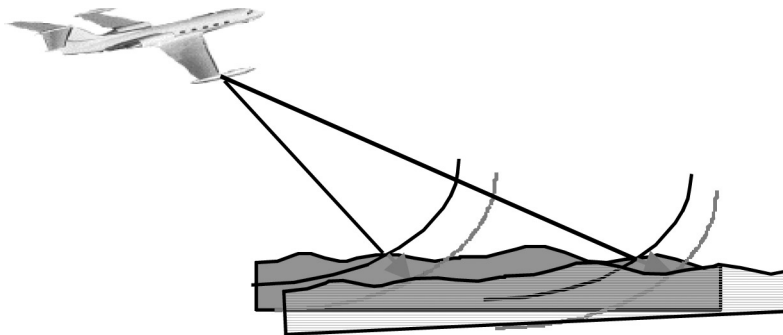

Figure 6.35 Range errors cause displacements along the line-of-sight. Points in the near range are displaced more vertically than horizontally whereas points in the far range are displaced more horizontally than vertically as illustrated above. See color plate in Appendix C.

Baseline Length and Orientation

As previously indicated, very accurate baseline knowledge is necessary to generate accurate topographic maps. Typically, the baseline length must be known to a fraction of a millimeter and baseline orientation angle to a thousandth of a degree. Surveying baselines to this level of

accuracy after installation on the aircraft is often difficult or infeasible. The phase center of an antenna, which is usually not the geometric center of the antenna, is the point on the antenna needed for baseline measurements. Analytical methods for determining the phase center from the physical and electrical properties of an antenna are not sufficiently accurate for interferometric applications. Baseline errors generate target location errors on the perpendicular to the line-of-sight as shown in Figure 6.36. The magnitude of the error depends on target location.
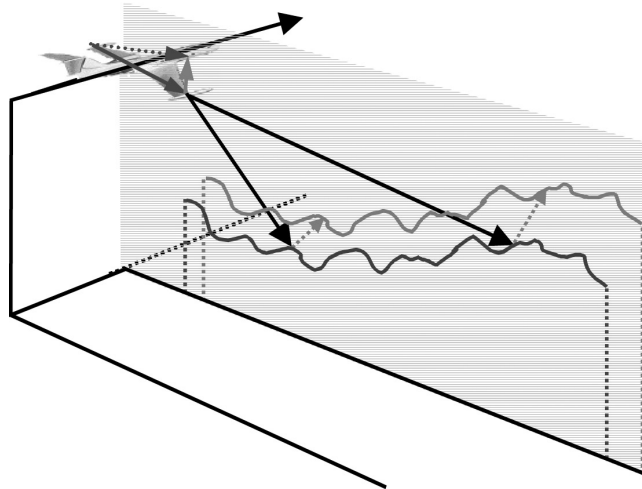
Figure 6.36 Baseline errors cause displacements perpendicular to the line-of-sight and the magnitude of the error is a function of cross track location. The correct baseline is the solid blue arrow on the aircraft, the red arrow is the baseline error (in this case mostly baseline orientation) and the dotted blue arrow is the incorrect baseline. The blue squiggly line represents topographic heights processed using the correct baseline and the red squiggly line the topographic heights with the incorrect baseline. The dotted red arrows point perpendicular to the line-of-sight from the correct to incorrect height. See color plate in Appendix C.

Phase

The differential phase between interferometric channels can have unknown phase delays due to variations in the phase center of the two antennas or from phase delays in the receiver chain. Temporal variation in either of these types of phase delay is tracked by introducing a signal of known relative phase into both channels and tracking the difference. The residual constant phase is then estimated as part of the calibration procedure. Phase errors translate into differential range errors that distort the observation triangle and lead to height errors in the topographic map as shown in Figure 6.37. The magnitude of the height error depends on range, and like baseline errors is perpendicular to the line-of-sight. A constant phase error causes a tilt and shift in the topographic map.

Another type of phase error occurs when reflected energy from the aircraft is received along with the desired signal from the surface as shown in Figure 6.38.

This type of phase distortion is referred to as multi-path and introduces a range varying sinusoidal phase error. Roughly speaking, the amplitude of the error depends on the magnitude of the reflected signal compared to the direct signal from the surface, and the frequency of the sinusoid depends on the distance from the antenna. Figure 6.39 shows the effect of multi-path on the TOPSAR system.
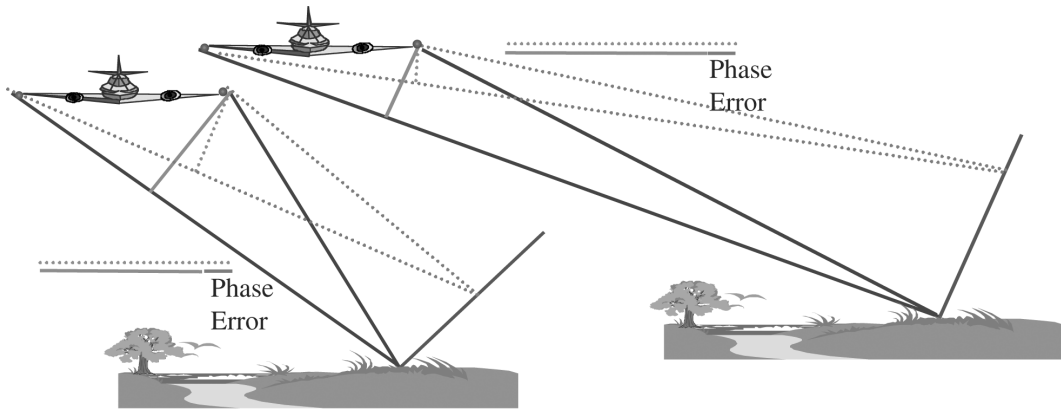
Figure 6.37 Phase errors viewed as differential range errors distort the interferometric observation triangle. The blue triangles represent the nominal interferometric observation triangles with the differential range indicated by the solid green lines. A phase error is introduced by changing the differential range by an amount equivalent to the length of the solid red line. The dotted red triangles show the resulting observation triangles. The position differences lie on a line perpendicular to the line-of-sight, the purple lines, and the amount of height error is range dependent as seen from the near range (left image) and far range (right image) examples. See color plate in Appendix C.
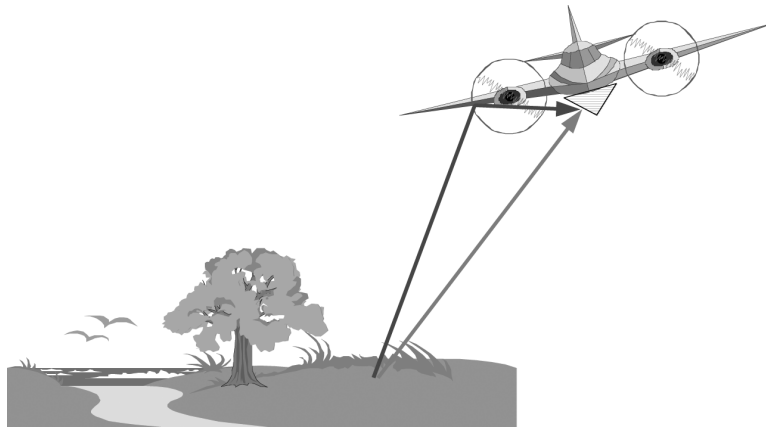

Figure 6.38 Signal reflected from the aircraft, blue line, that is received at the same time as the direct signal return from the surface, red line, introduce a range varying phase error. See color plate in Appendix C.
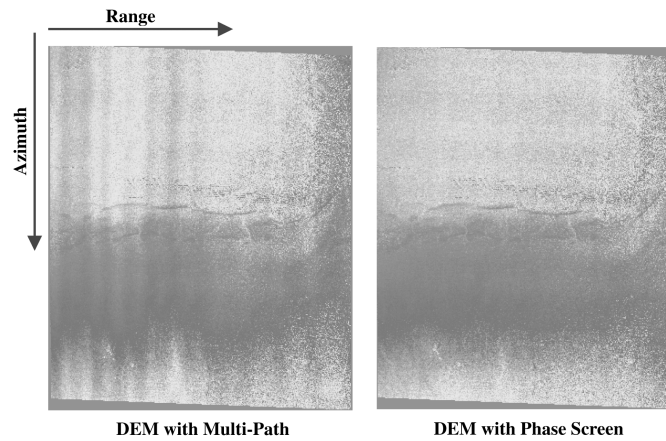

DEM with Multi-Path   DEM with Phase Screen

Figure 6.39 Topographic map of Mojave Dessert, CA created with and without using a phase screen. Note the cross track ripples 1-10 m in amplitude in the map without the phase screen characteristic of multi-path. See color plate in Appendix C.

Chapter 6   179

Radiometric Calibration

Although there is no radiometric accuracy requirement imposed on the imagery for purely DEM applications of IFSAR data, most providers radiometrically correct imagery for antenna pattern and range effects. Prior to mosaicking strip imagery, additional radiometric balancing of the image data to reduce swath-to-swath brightness variations caused by drift in radar system parameters or radar system parameter changes may be necessary. Imagery may be used to aid in breakline determination, terrain use classification and identification of potential water constriction features.

Calibration Site and Procedure

Determining the calibration parameters requires a site with an arrangement of radar identifiable fiducial points (surveyed corner reflectors) over which repetitive overflights are made. In addition, a site with a high accuracy DEM covering an area larger than the cross track direction of the swath and of sufficient size in the along track direction is needed to determine an elevation angle dependent phase correction. Described below are the key calibration parameters, how they are determined, and their effect on DEM accuracy.

To separate the effect the various calibration parameters have on height error, the differing cross track dependencies of the error sources is exploited. A site, preferably with little or no vegetation, is prepared with radar identifiable fiducial points arranged in the cross track direction as shown in Figure 6.40.
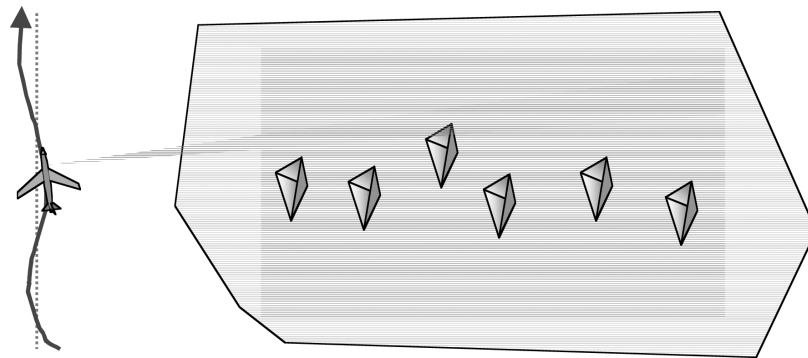

Figure 6.40 IFSAR calibration site is equipped with an array of corner reflectors deployed across the imaging swath of the radar (shown in green). A high accuracy DEM covering the range swath (shown in blue) may be co-located with the corner reflector array or at a different site. Multiple lines are flown at the corner reflector array, and the DEM location if different, in order to determine the calibration parameters. See color plate in Appendix C.

There are several ways of making radar identifiable fiducial points, however the most popular means are passive devices known as corner reflectors. Corner reflectors are metallic objects, shaped either as trihedrals or dihedrals (hence the name corner reflector), that show up as bright objects in radar images. Moreover, trihedral corner reflectors behave as point scatterers, that is the reflected energy acts as if it emanates from a single point (the apex), thereby providing a well defined point from which range measurements may be calibrated. Corner reflector locations are GPS surveyed (and often monumented) to centimeter accuracy. Examples of both types of corner reflectors are shown in Figure 6.41.

Calibration begins with repetitive overflights of the calibration site or sites exercising all the IFSAR mapping modes and configurations. Several flight altitudes may be flown for each mode or configuration to verify stability of the calibration parameters or to generate altitude dependent corrections. The data are first processed to form slant range images. Corner reflector locations, range and along track coordinates, in the slant plane imagery can be predicted from the surveyed locations of the corner reflectors and platform ephemeris data. The predicted range is compared with the measured range and the difference forms the common range delay correction. Range pixel location can be determined to better than a tenth of a pixel by oversampling the slant plane

Figure 6.41 The two types of corner reflectors normally deployed for SAR calibration are a trihedral shown in the left of the figure and a dihedral shown in the right of the figure. Physical size of a corner reflector used for calibration is a function of the wavelength, radar transmit power, antenna size and range. The trihedral is this figure is approximately 2.6 m measured along a diagonal edge and the dihedral is about 2 m high.

imagery. Because range measurements to the two interferometric channels may differ, a differential range correction is computed, by measuring range offsets between the two channels. Differential range measurements are accurate to better than a hundredth of a range pixel and insure proper range registration of the channels during interferogram formation.

After determining the common and differential range corrections, the data are reprocessed and strip map DEMs and orthorectified imagery are generated. Planimetric positions of the corner reflectors are measured using oversampled orthorectified imagery. The height of the corner reflectors is obtained by interpolating the interferometric DEM to get the height at the measured planimetric location of the corner reflector. By comparing the surveyed 3-D locations of the corner reflector array to the interferometrically observed positions, correction estimates for baseline length, baseline orientation angle, and phase are made via a least squares technique. Finally, the high accuracy DEM is used to generate a phase screen that provides elevation angle dependent phase corrections for effects such as multi-path and switch leakage. Radiometric calibration of the imagery using corner reflector brightness can be done at this stage if desired or required for the system.

Checking Calibration

Calibration of the IFSAR system is usually done on a regular basis or if the system has undergone any significant change that may effect the calibration. The interval between calibrations depends on the system and its overall stability. Calibration may be linked to major system deployments or occur on a regularly scheduled basis. Periodic checks may be made by deploying a small number (3-4) of surveyed corner reflectors at a site and verifying planimetric and vertical accuracy or comparing height measurements with other data sources or equal or better quality. Kinematic GPS surveys, static GPS survey points, lidar or photogrammetric DEMs provide excellent sources to verify calibration.

PLANNING CONSIDERATIONS

Careful planning and execution of IFSAR data collections are needed to ensure that customer requirements are met and to avoid costly operational errors. Planning considerations can be divided into four phases: requirements definition, mission planning, site operations and data collection. The basic aspects for each planning phase of an airborne SPI data collection are described. Many of these same considerations equally apply to spaceborne and RPI data collections.

Requirements Definition

In the requirements definition phase, the customer and data provider agree upon the overall objectives for a project. First, the customer provides the data provider a description of the site to be mapped, planned use of the data, and their expectations for data quality. The data provider evaluates whether the customer's expectations and planned use of the data are realistic and provides recommendations to the customer as to whether to proceed or not. Customers that have not worked with IFSAR data may be shown sample products to aid their assessment of the applicability of IFSAR data to their project.

Next collection requirements for the region to be mapped are established. Boundaries of the site or sites to be mapped are identified geographically. The customer specifies the desired mapping accuracy. Accuracy requirements may vary spatially, for example flat areas may require one level of accuracy whereas mountainous or vegetated areas may have another. The customer specifies special operational logistics, for example required time of day or year, coordination with ground activity at the site, or coordination with other sensor collections. Mission timing can be critical to obtaining maximal information from IFSAR derived DEMs. Time of day or year may be specified to coincide with low tide in littoral regions or leaf-off conditions in deciduous areas. Mapping in agricultural areas might be linked to a specific time in the growing season or to the post harvest period to avoid mapping seasonal crops. Depending on the wavelength of the radar, it may be necessary to avoid collections during times when the ground is covered by snow levels the radar is unable to effectively penetrate. Coordination with ground activity may be needed if the customer has need for IFSAR data contemporaneous with other activity at the site, or they may wish to deploy their own ground control (e.g. corner reflectors) for the data collection. The amount of allowed voids and multiple passes should be specified. Again these requirements may vary spatially to coincide with areas of greater interest or greatest need. For example, urban areas may need to be mapped on two or more passes from different look direction to prevent holes from shadow and layover in the map products.

IFSAR systems generate a number of data layers in addition to DEMs such as orthorectified SAR imagery and height error maps. Desired output products from the collection must be specified. The customer specifies the datum, geoid and map projection. If the data provider does not support the desired datum, geoid or map projection then the customer may select alternates that can be converted to the desired data representation. With the proliferation of data formats and storage media, it is essential that the customer and data provider agree upon format and delivery media.

To aid in mission operation the customer and data provider should review existing data at the site. This may include DEMs, paper maps, or other relevant reports that provide insight on restrictions or problems affecting either ground or air operations. Finally, a careful review of the expected results between customer and data provider can help avoid mission replans that may increase cost or cause delay in schedule.

Mission Planning

The mission planning phase transforms the data collection requirements into a data collection plan that includes flight lines, instrument parameters, and required coordination activities. A review of overall mission logistics determines the tasks that must be accomplished and the items that must be scheduled, coordinated and tracked. Based on customer input and aircraft availability, the data flights are scheduled. Usually, flight operations are scheduled with contingency days which can be used to recover data lost due to equipment failure or other unforeseen events.

A suitable base of operations is needed for sites outside the data provider's home base operating sphere. Locating an airport within the aircraft's operating range to the site and with runway and hangar facilities equipped to support the data provider's aircraft is one of the first priorities. Additional facilities, possibly remote from the airport, include hotel and meeting areas near the site to support ground activities. A check is made for existing ground control available to support DGPS data collection, and if nothing suitable is located, provisions for establishing control are arranged. The amount of coordination required for spectrum use depends on the operating frequency of the data provider's IFSAR system and the country where the site is located.

Data providers have a great deal of flexibility in scheduling flight lines to generate a DEM having the required posting, accuracy, and data voids based upon their system's operating parameters. An analysis of the project area, project requirements, topography, proximity to restricted airspace, flight altitude, radar parameters and other factors will determine the flight path configuration. The spacing between flight lines will depend on the desired amount of swath overlap between adjacent mapping strips and the steepness of the terrain. Multiple incidence angles are often used in steep terrain in order to fill data gaps caused by radar shadow or layover. Missions consisting of multiple parallel flight tracks should include crossing tracks spaced roughly 10 swathwidths or less apart to help maintain control between flight lines as shown in Figure 6.42.
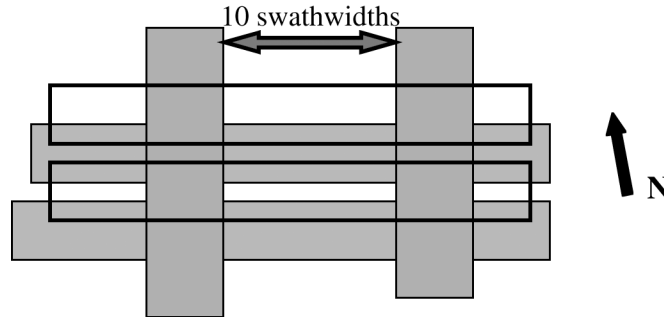

Figure 6.42 IFSAR providers need to plan sufficient overlap between adjacent swaths to avoid data gaps due to terrain effects and should allow for crossing swaths to help maintain control between parallel mapping swaths.

Planning to avoid significant shadow and layover dropouts in areas with significant relief is required. An image mask indicating the predicted image voids for each strip can be generated using existing DEMs such as those available from the USGS. Although the accuracy of the predictions will vary with the quality and post spacing of the planning DEM, this exercise helps verify radar command parameters are set properly. Data masks are generated for each flight line individually and mosaicked together to predict the amount and location of voids in the final product. Figure 6.43 shows a mosaic of the predicted data voids and overlap between flight lines for a TOPSAR data collection over Orange County, CA. Adjacent to the prediction mosaic is shown the mosaicked image and DEM for that collection. Tools such as the one illustrated help ensure both the customer and data provider that the planned data collection will meet coverage requirements. At this point the customer gives the final approval to proceed with mission.
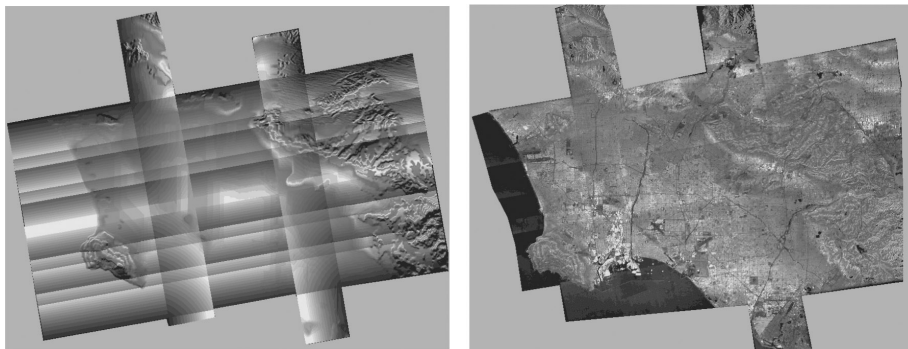

Figure 6.43 The left figure is a mosaic of image masks from 8 flight lines used in planning an Orange County data collection. Visible is the planned overlap of a quarter of a swath (3 km) between the 6 adjacent east-west flight lines and the 2 orthogonal flight lines used to maintain control. The right figure is a mosaic of the processed TOPSAR data from the Orange County collection. Each color cycle used to depict elevation contours represents 100 m of elevation change. Brightness in the image mask mosaic is derived from a shaded relief of the USGS DEM used to make the mask whereas in the TOPSAR mosaic it is the radar backscatter. See color plates in Appendix C.

Chapter 6   183

Site Operations

Site operations are the initial steps in executing the mission plan. A pre deployment visit to the airport, DGPS base station, base of operations and the site are made to confirm mission planning assumptions are valid. Major variances with the planning assumptions can lead to modifications to the mission plan. All necessary paperwork to conduct flight and ground operations such as visas, flight permits, data export licenses, landing authorizations and spectrum allocation are obtained and verified. A pre-deployment check of the aircraft, radar and ground support equipment is conducted to verify everything is working properly.

Equipment and personnel that must be on site prior to data collection are transported to the base station. Equipment may include flight spares, additional DGPS stations and corner reflectors. The status of activities that need to be completed or initiated prior to data collection such as corner reflector deployments or other ground truth activities are checked. At this point the aircraft and flight crew are deployed to the site and a final check of flight systems is conducted. Agencies such as Air Traffic Control (ATC) are contacted and permission for flight operations confirmed. Finally, the aircraft and ground crew review pre-mission contingencies and mission abort criteria.

Data Collection

If all mission operations could be executed exactly as planned, site operations would mark the end of planning considerations. However, events unforeseen during the mission planning phase can force alteration to the planned data collection strategy. Briefly, a data collection proceeds as follows. A pre-flight briefing between the aircrew, radar operator, and ground crew is conducted the day before or on the day of the data collection to make sure there have been no changes to plans and to coordinate with any other ground truth or sensor collections that may be taking place. The DGPS is deployed to the DGPS base station and data collection is begun approximately one hour prior to takeoff. The aircraft and radar systems go through a pre-flight checklist. Radars with Built-In-Test (BIT) equipment go through their pre-flight sequence. After takeoff and arriving at the site, collection of the planned datatakes commences. The radar operator monitors radar, INU and DGPS, and other metrology systems to check for any operating anomalies. After the mission a post flight briefing is conducted to note any anomalies with the air or ground operations. If warranted, alterations to the mission to facilitate operations or correct deficiencies are made. Data is periodically forwarded to the processing center for further checks of data integrity and system health. This continues until the mission is complete.

COMPARISON WITH OTHER TECHNOLOGIES

Photogrammetry and lidar systems are other remote sensing technologies designed to make topographic measurements (see Chapters 5 and 7 for a detailed discussion of these sensors). Each type of sensor is sensitive to different aspects of the surface under observation and therefore measures height differently depending on surface type and ground cover. All of the above sensors make height measurements that depart from an "idealized height sensor" that gives the height measurement at precisely one point. Only for simple surfaces or after appropriate post processing of the data can the height measurements of the three types of sensor be directly compared with point measurements like those obtained by DGPS surveys.

The desired elevation measurement is application dependent. Flood plain applications require DEMs to have all vegetation and buildings removed, and water constriction features such as bridges, fences and power poles edited from the data. However, for flight obstruction or forest mapping it is desired to leave some or all of the elevations unaltered. Each of the different sensor technologies has strengths and weaknesses depending on the desired height measurement for a particular application. In fact, a synergistic combination of measurements from two or more of the above sensors can produce the best possible product.

As the variety of IFSAR, lidar and photogrammetric sensors is quite numerous, and performance parameters continuously improving for all three types of sensors, only very general comparisons of the sensor characteristics are presented[10]. The primary characteristics that distinguish the sensors and their height measurements are shown in Figure 6.44. Lidar[11] and IFSAR systems are active sensors supplying their own illumination source, IFSAR and photogrammetric systems are imaging sensors, and lidar and photogrammetric are optical sensors.
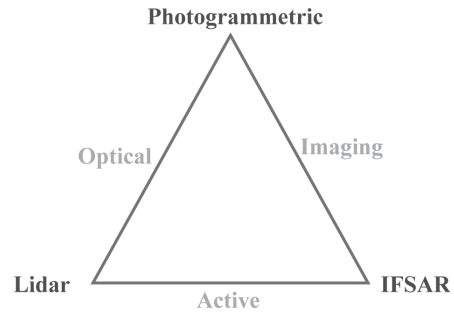
Figure 6.44 Figure showing the primary sensor characteristics shared by the three pairs of sensor combinations.

Photogrammetry

Photogrammetric sensors, like IFSAR systems, generate both imagery and height data and have been operated on both airborne and spaceborne platforms. Unlike aerial or spaceborne photogrammetry, IFSAR missions can be flown without regard to sun angle. Flights may take place at night or in conditions of inclement weather provided the conditions are such that the image formation process is not degraded. Airborne optical cameras continue to generate extremely fine resolution (often sub-meter) imagery without the troublesome layover and shadow problems of radar. However, radar interferometers are proving to be a cost-effective method for wide area, rapid mapping applications, and do not require extensive hand-editing and tiepointing. Additionally, because IFSAR systems often fly at greater altitudes, they can operate in congested air-traffic corridors that are often difficult to image photogrammetrically. Mapping in tropical regions that are often cloud-covered can be done more reliably with IFSAR systems that penetrate clouds. Urban mapping is a challenging venue for mapping by IFSAR systems due to the extremely complex scattering environment. Although some high resolution systems have shown promise for urban mapping, photogrammetry still has inherent advantages for this application.

Densely vegetated surfaces can be problematic for both sensors if bare surface elevations are desired. Photogrammetric true ground surface heights can only be obtained if sufficiently large gaps are present in the canopy. These points, usually determined manually, are then extrapolated to other portions of the canopied area to produce bare surface height maps. Heights measured by IFSAR systems are reflective surface heights and can lie anywhere within the canopy. Longer wavelength systems penetrate deeper into the canopy but the exact location within the canopy corresponding to the height measurement is not easily determined. IFSAR correlation has information about the vertical structure of the canopy and has the potential of providing corrections to measure bare surface elevations [Hagberg et al, 1995], [Rodriguez et al, 1999] and [Hokeman and Varekamp, 2001].

Unlike photogrammetric and lidar systems, IFSAR systems can generate height error maps on a pixel-by-pixel basis [Hensley and Webb, 1994]. These images provide an estimated relative statistical height error as described earlier. These products are extremely useful for ascertaining whether an IFSAR derived DEM is suitable for a particular mapping application and for locating problematic regions within the DEM. Figure 6.45 shows a height error map of Long Valley, CA made using the TOPSAR system and a comparison with measured statistical height errors from kinematic GPS measurements.

---

[10] Many detailed sensor comparisons between sensors have been made like the ones discussed in [Madsen, 1993], [Hensley and Webb, 1994] and [Mercer et al, 1999].

[11] Previously, operating commercial lidar systems did not record the reflected lidar signal level that could be used to form a lidar image. However, intensity images are now being offered by lidar vendors, as explained in Chapter 7.
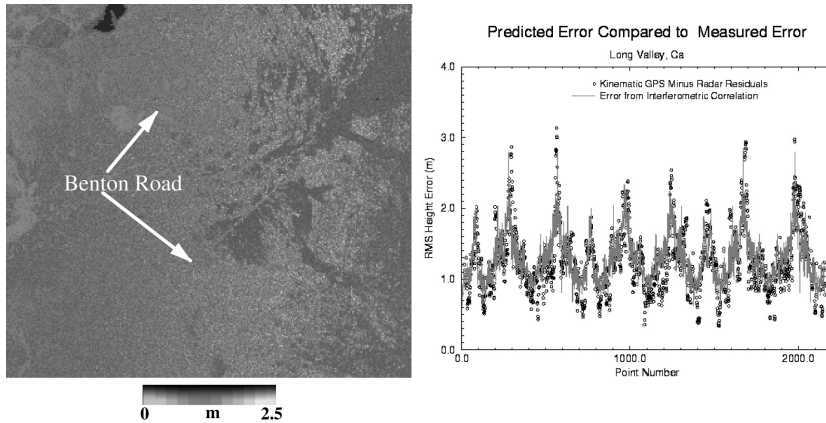
Figure 6.45 Local height errors computed from the interferometric correlation data were compared with kinematic GPS measurements by computing the "local" RMS height difference between the TOPSAR and GPS measured heights along Benton Road in LongValley, CA. See color plate in Appendix C.

Lidar

Lidar like IFSAR is an active sensor providing its own illumination and similarly records the time delay between transmit and receipt of reflected signals from the surface. Employing a very narrow beam so that the projected footprint on the ground is typically 10 meters or less from space (several feet from airborne sensors), lidar systems obtain one or more height measurements per pulse. The number of height measurements is dependent upon the vertical structure of objects within the beam and the type of lidar system as shown in Figure 6.46. Some lidar systems are equipped to only record a single time delay per pulse whereas other systems record time delays for multiple samples exceeding a signal level threshold. By scanning cross track to either side of the nadir point of the aircraft and rapidly pulsing the laser reasonable mapping swaths are obtained. Operating at optical instead of microwave frequencies, lidar systems do not penetrate clouds and other atmospheric obscurants.
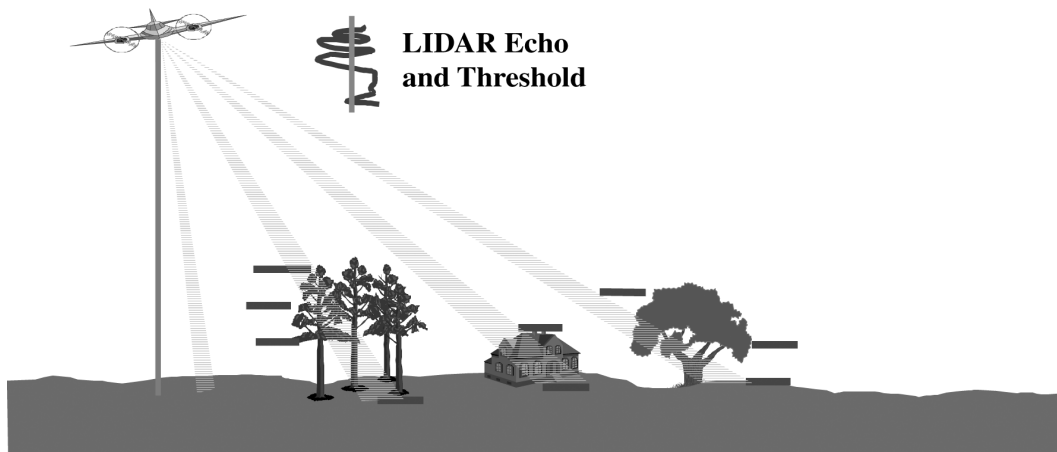

Figure 6.46 Lidar systems like IFSAR systems are active sensors that measure range. Liears use narrow scanning beams to localize their targets spatially. Some lidar system measure the height of multiple returns (denoted by blue bars next to object in scene) exceeding a specified threshold (sample echo in blue with threshold in green next to plane) thereby providing additional information about the vertical structure of objects in the scene. See color plate in Appendix C.

Unlike IFSAR systems lidars are not imaging sensors. Applications where contextual information that is not easily derived from height data alone favor IFSAR and photogrammetric mapping sensors. Classification studies and resource inventory surveys are examples where imagery plays a vital role in separating and identifying vegetation and crop types, geologic structures, and various anthropogenic uses. Water body mapping and delineation is often possible with IFSAR systems depending on the frequency of operation and the roughness of the water body surface, whereas lidar systems do not obtain good height measurements over water.

Lidar systems have become the sensor of choice for mapping vegetated regions when elevation measurements beneath the canopy are needed. True ground surface elevation measurements are obtained after a post processing step to insure the reflective surface does not arise from within the vegetation canopy. As previously noted, heights measured by IFSAR systems are reflective surface heights and can lie anywhere within the canopy, but with proper frequency selection and use of correlation data has the potential of providing corrections to measure bare surface elevations. Larger swaths possible with IFSAR mapping systems can substantially reduce the time to collect data over large areas.

POST PROCESSING

Processing and post processing of IFSAR data affect the accuracy and quality of final map products. The division between processing and post processing is somewhat arbitrary, however for the purposes of this chapter post processing will be defined to begin after the interferometric phase is transformed to a position and elevation measurement. Many aspects of IFSAR post processing are nearly identical to standard photogrammetric or lidar post processing. The type and amount of post processing is application dependent and is tailored to meet specific user requirements. In this section some of the most common IFSAR post processing steps are described.

Regridding

Critical to understanding the final DEM is the posting to smoothing window ratio. Smoothing of the interferometric phase measurements is done to reduce phase noise and aid in the unwrapping process. Typically this involves spatially averaging the phase over a window by an amount that is set by the processor operator. This window is often larger than the post size of the DEM. Thus the effective resolution of the DEM may be less than post size depending on the spatial frequency spectrum of the underlying topography.

Unwrapped phase measurements lie on a uniform grid in range and azimuth, however the position measurements determined from the phase measurements are distributed unevenly with respect to the processor ground projection. To obtain an elevation map on a uniform ground projection grid the data is interpolated or resampled to the desired posts in the regridding process. The regridding algorithm employed affects the resulting height accuracy and spatial resolution of the IFSAR map products. Regridding algorithms include the simple nearest neighbor algorithm where the point closest to the desired post within a specified radius is used to more sophisticated algorithms such as surface fitting or more general interpolation algorithms. Adaptive regridding algorithms adjust the smoothing spatially based on the amount of topographic relief with more smoothing done in flat areas to reduce the height noise and less smoothing done in areas with substantial relief to maintain spatial resolution.

Map Mosaics

Mosaicking is the process whereby multiple images and/or DEMs are merged into a single image and/or DEM with a common datum, map projection and data format. The mosaicking process may involve DEMs in multiple coordinate systems that can be derived from multiple sources (e.g. interferometric, USGS, DTED, photogrammetric or lidar), have different data types (e.g. floating

point, integer) and have different units (e.g. m, ft). Mosaicking of elevation data is inherently a 3-dimensional process and uses algorithms capable of manipulating and combining 3-dimensional data sets in order to produce high quality seamless mosaics. The mosaicking process can be divided into four steps: determination of the data sets to be mosaicked, finding ground control and tie points, mathematical adjustment of the data sets based on the tie and ground control point data, and combining of the multiple observations into a seamless map product.

If geolocation of the individual map components is sufficiently accurate, mosaicking is done via dead reckoning, that is placement of pixels in the final mosaic is based on the *a priori* positioning data of the individual components. A combination of ground control and tie points can be used to improve absolute and relative geolocation accuracy. Ground control points are points in the component data sets that are identified with external data having known absolute positions. These data are used to remove both relative and absolute positioning errors depending on their distribution within the data sets. Typically, these points are generated from corner reflectors or from manually identified points. Tie points are points identified to be the same point in two or more of the component data sets. These data can be used to remove relative position errors between the data sets, but do not provide absolute position information. Tie points are generated using automated matching algorithms to match either the imagery or elevation data.

Before the data can be combined into a final mosaic, a mathematical framework that includes the required coordinate conversions and position corrections based on tie and ground control point data must be established. The model may be sensor based if only one type of data is to be combined (e.g. IFSAR or photogrammetric data) or based on a more generic error function such as affine transformations[12]. Regardless, care must be taken to avoid fitting for parameters in the model that are not well constrained by the distribution of tie and ground control points.

The final step in the mosaicking process interpolates the individual data sets into the map mosaic coordinate frame and combines what may be multiple observations into the final map product. Combining multiple data sets from the same sensor or from multiple sensor seamlessly uses a smooth blending from one data set or combination of data sets to another called feathering. Feathering adjusts the relative weighting of the different data sets over a specified distance to smoothly transition from one data set or combination of data sets to another. The feathering weights may be further adjusted to reflect the height accuracy of the individual points by incorporating the height covariance estimates determined from the correlation measurements. In this way posts in the final map mosaic favor the most accurate IFSAR mapping data.

Datum/Geoid and Map Projection

The user specifies the desired datum, geoid and map projection for the final DEM. During the mosaicking process the individual IFSAR mapping strips are projected into a common coordinate system that is normally the desired user map projection and datum thereby avoiding unnecessary data interpolations. Correcting the heights to the desired geoid can be part of the mosaicking process or done in a separate post processing step.

Hole Fill

Data gaps from layover, shadow or low signal regions may be present after mosaicking is complete. Filling these data gaps may be required for some applications. There are three basic methods used to fill gaps in the final DEM. Data may be specially acquired over the gap regions, data from alternate sources may be used, or analytical methods for filling gaps may be employed. Specially acquired data to fill residual gaps is the most expensive means of filling gaps in the DEM and may require a delay in product delivery to allow for data collection and processing. This

---

[12] Affine transformations are linear transformations plus a translation. Affine transformations can be decomposed into rotational, scale, skew and translation components and for most sensors small errors are well modeled by these terms.

option has the benefit of maintaining uniform quality data throughout the DEM but is usually warranted when there are excessively large data voids in critical portions of the DEM. Data from previous data collections or other data sources (e.g. USGS DEMs) may also be used to fill in gaps in the data. These data in general may not meet the same accuracy or resolution requirements of the IFSAR data, however alternate source data often proves adequate for small gaps. By incorporating these alternate sources during the mosaicking process, a seamless final product is achieved, provided there has not been extensive change to the topography between the time of the IFSAR data collection and the time the alternate source data were acquired. A myriad of algorithms is used to analytically fill gaps in topographic data. Surface fitting, kriging methods, and polynomial interpolators are among the most commonly employed algorithms for hole filling. The choice of algorithm depends on the size of holes to be filled and the intended application for the DEM.

Data Editing

Data editing is used to correct errors in the DEM detected during the quality control process or to manipulate height values so that they conform to a user prescribed mapping standard. Unwrapping errors occur when an incorrect multiple of 2π is added to the interferometric phase measurement. This results in the IFSAR elevation measurements being too high or too low by a multiple of the ambiguity height, a quantity that is determined from the interferometric system parameters and mapping geometry. Unwrapping errors are detected and edited from the DEM by searching for height discontinuities that are multiples of the ambiguity height. Spikes and wells are isolated points in the DEM whose elevation differs from surrounding heights by an unphysical amount. These points are edited from the final DEM and marked as data voids or filled in using a combination of the surrounding elevation values. Some map products (e.g. DTED products) require that water bodies have single elevation value. IFSAR DEMs over water are usually noisy and have intrinsic height variation that depends on the amount of thermal noise. Water body editing consists of identification of the water body and setting the elevation to the desired value. Water body identification using IFSAR data is a difficult problem and is a significant portion of the editing process.

Vegetation Removal

Applications that require bare surface DEMs need to have IFSAR reflective surface elevation measurements corrected to bare surface elevations. Correction of reflective surface elevation measurements is called vegetation removal. Vegetation removal involves identifying vegetated regions and then correcting the elevation measurements to the bare surface. Identification of vegetated region uses combination of imagery, elevation measurements and correlation data. Correction to bare surface elevations may employ algorithms similar to lidar and photogrammetric sensors where elevation measurements that penetrate to the bare surface are used in combination with surface fitting algorithms to make elevation adjustments. More sophisticated algorithms that use the image brightness, correlation and elevation measurements along with a model of the vegetation are now being employed by some IFSAR sensors for vegetation removal.

Derived Products

In addition to the IFSAR image and DEM products, several derived products based on the IFSAR data may be generated during post processing and provided to the customer. Classification maps that delineate water body boundaries, urban and vegetated areas, as well as other classes are possible using IFSAR data or IFSAR data in combination with other sources such as Landsat imagery. Slope and curvature maps necessary for hydrological and seismic hazard assessment and landslide potential studies can be derived from the height and height error maps. Semi-automated road identification based on a combination of IFSAR imagery and elevation measurements can provide an updated cartographic layer for map generation. Breakline identification and water body constriction removal are post processing steps usually required in flood plain mapping applications.

QUALITY CONTROL

Quality control is a task or series of tasks that scrutinizes all, or a sample, of the IFSAR products issued during, or at the end of, the IFSAR map generation process in order to ensure that the final product meets or exceeds requirements [Ackerman, 1994], [Burrough, 1986] and [Positional Accuracy Handbook, 1999]. This scrutiny involves a combination of review, inspection and quantitative measurements, against well-defined criteria that are outlined in references. Additional quality controls determined by the data provider are used for other map products such as SAR imagery and other IFSAR specific derived products. Many data providers certify their QA/QC processes to the ISO-9002 standard. An overview of some of the standard qualitative and quantitative quality control procedures is presented in the following sections.

Visual Accuracy Checks

Visual quality control begins by looking for gross processing errors associated with incomplete phase unwrapping, large spikes and wells, large tilts on water bodies and features that seem out of place. The maximum and minimum elevations in the IFSAR DEM are compared to the maximum and minimum values represented by contours or spot elevations available on the most recent available map. A check for completeness in the project size and for continuity along mosaic seams and data gap boundaries is also made. Overlay the IFSAR map products on available map data to check if geo-referencing is correct. Spot check selected pixel values such as corner and center pixel values against heights on published maps. Use a DEM viewing workstation with the appropriate soft-ware tools to aid in the identifications of blunders such as spikes and holes. Blunders are gener-ally identified through a combination of color banding of elevation contours, stereoscopic viewing using anaglyphic filters, shaded relief enhancements and use of histograms. Artifacts identified during the visual accuracy checks are documented and quantified noting the location and source, for example: terrain masking, radar shadow, DEM sub-patch boundary, land/water boundary, vegetated regions, wind motion, or other factors.

Ground Truth

Quantitative assessment using ground truth data is an important component of the quality control procedure. A selected set of ground control points, typically greater than 20 for any region or sub-region to be tested, is compared with the corresponding IFSAR generated height measurements. For a rectangular area that is believed to have uniform positional accuracy, check points may be distributed so that points are spread at intervals of at least 10% of the diagonal distance. At least 20% of the points are to be located in each quadrant. The independent source of higher accuracy shall be of the highest accuracy feasible and practical to evaluate the accuracy of the IFSAR data. To make a rigorous accuracy assessment usually requires truth data that is three times more accurate than the product tolerance. Each checkpoint must be well defined (NMAS, ASPRS and NSSDA mapping standards – see Chapter 3) in the context of the image resolution, resolution and features that are present. A well-defined point represents a feature for which the horizontal position is known to a high degree of accuracy and for which the absolute position with respect to the map product geodetic datum is known. Kinematic GPS measurements taken along major highways and trunk roads provide excellent data sets for quality control and accuracy assess-ments. Kinematic GPS transects should be collected away from urban areas where multi-path in the radar and kinematic GPS data is often problematic.

Height accuracy is slope dependent for IFSAR mapping systems. Accuracy assessments grouped according to slope magnitude ease the comparison with the National mapping standards. The National Map Accuracy Standards (NMAS) and the ASPRS accuracy standards for large-scale maps states that for the purposes of checking elevations the map position of the ground point may be shifted in any direction by an amount equal to twice the limiting RMSE position accuracy. Implicitly this allows for spatially varying height accuracy that may be slope dependent. Evaluating the accuracy in different sub-regions grouped by slope and using the standard specified above gives a better overall assessment of map accuracy.

Height Error Map Accuracy Analysis

One of the valuable map products generated by IFSAR mapping systems is the local statistical height error map generated from the correlation measurements using Equations 6.8 and 6.9. The error map provides the user with a point by point assessment of the vertical accuracy of the DEM. Evaluation of the height error map accuracy is done using areas of bare surface. The height error map accuracy is assessed using the local relative height error at a point p, σ_{h_p}, which is defined as

$$\sigma_{h_p} = \sqrt{\frac{1}{\#(B)} \sum_{q \in B} \left(h_{r_q} - h_{t_q} \right)^2 - \left[\frac{1}{\#(B)} \sum_{q \in B} \left(h_{r_q} - h_{t_q} \right) \right]^2} \qquad (6.12)$$

where h_r is a radar height value, h_t is the corresponding ground truth height value, B is the set of points in a neighborhood of the point p (to be defined), and #(B) is the number of points in B. B should be a box centered at p with size equal to 5 pixels as shown in Figure 6.47. The estimate of σ_{hp} should be considered valid if and only if #(B) is greater than or equal to 10.
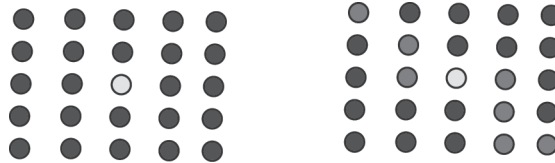

Figure 6.47 This figure shows the neighborhood, B, about a point, p (yellow circle), where the local statistical height accuracy is being measured. A sufficient number of control points (shown in red) should be present in order to make a valid assessment. See color plate in Appendix C.

Control points are usually derived from either kinematic GPS measurements or a high accuracy photogrammetric or lidar DEM with relative height accuracy at least three times better than the expected IFSAR mapping accuracy. Height error estimates are assumed valid if 90% of the points have a local statistical height error that is within 20% of the IFSAR predicted statistical height error.

USER APPLICATIONS

Fine resolution topographic measurements have applications throughout the commercial, civilian, and military sectors. Applications include, for example, land slope stability and land-slide characterization, land-use classification and change monitoring for agricultural and military purposes, flood plain and hydrological modeling, littoral zone mapping, and archeological and geological applications. The accuracy and resolution depend on application, and a number of technologies are usually available that can meet any particular application requirements. The ability to generate accurate IFSAR DEMs at regional or global scales quickly and at a reasonable cost has seen the rapid infusion of this technology into a variety of applications.

Hydrology

The insurance industry as well as local and national governments have become increasingly concerned about proper risk assessment associated with flooding. Risk assessment is needed for flood warning, flood plain control and financial liability studies. Flood plain mapping and risk assessment uses a combination of topography and surface cover type along with propagation models to determine depth of flooding. Airborne derived IFSAR DEMs with the combination of accuracy and resolution and cost have proved ideal for regional flood risk assessment as has been shown in several studies both in the United Kingdom [Galy and Sanders, 2000] and in the United States.

---

[13] Mapping water body surfaces is usually only possible for higher frequency systems (C-band and above) and when there is sufficient wind or current to make the water appear rough at the imaging wavelength.

Littoral Zone Mapping

Littoral zone mapping is an area where IFSAR mapping is playing an increasingly important role because it maps from the near shore regions out onto the water surface[13]. Photogrammetric and lidar systems have greater difficulty mapping these regions because neither type of system makes height measurements over water bodies. By mapping at low tides IFSAR systems should provide some of the most complete and detailed maps of the littoral zone.

Seismic Hazards

Slope and along-slope and cross-slope curvature estimates are needed for slope hazard analysis. Special care must be taken in computing slope and surface curvature from interferometric DEMs because point-to-point height noise can be comparable to a significant fraction of the post spacing. Studies have shown that when this is taken into account, IFSAR derived DEMs improve classification of areas of landslide induced seismic risk [Real et al, 1997].

Urban Mapping

Urban mapping varies from the relatively low density and simple structures of a suburb to the extremely complex and high density environment of a modern major city. Multiple scattering, shadow and layover make urban mapping a challenging application environment for IFSAR systems. High resolution airborne IFSAR systems have shown some utility for this application particularly in medium to low density urban areas [Mercer and Gill, 1998]. System resolution and the degree of algorithm optimization for urban environments greatly affect the achievable mapping accuracy.

Archeology

Understanding where, how and when ancient civilizations modified and controlled their physical environment is an aspect of archeological research where SAR and IFSAR systems have made important contributions. Multiple frequency observations that penetrate into dense vegetation coupled with accurate topographic information is providing archeologists with unique regional scale observations of ancient sites such as Angkor Wat in Cambodia and the Great Wall in China. Because of the unique perspective SAR and IFSAR systems can provide, the use of these data in future investigations is expected to increase.

Vegetation Mapping and Land Use Classification Maps

The use of interferometry for land use classification and vegetation parameter determination is a rapidly expanding area of research. The use of multi-frequency IFSAR systems that exploit the relative penetration into the canopy, and the use of interferometric correlation which is sensitive to the vertical structure of the canopy, have shown great promise for extracting canopy parameter elevations [Hagberg et al, 1995], [Rodriguez, Martin and Michel, 1999], [Hokeman and Varekamp, 2001] and [Hensley et al, 2001]. Land use maps that have classification accuracy in the 90% level have been demonstrated using data from airborne IFSAR systems [Rodriguez, Martin and Michel, 1999] although significant ambiguities were observed under certain conditions. Specifically, problems arose due to the sensitivity to the absolute calibration of the radar backscatter and from changes in backscatter as a function of incidence for the same ground cover type. Using multi-frequency, multi-temporal or other optical data sources can significantly reduce classification error.

Geology

Topographic maps have traditionally played an important role in geological applications. IFSAR system height and image data can simultaneously provide topographic information at two scales. Using the topographic data directly, topography at the DEM posting provides information about geologic structures such as faults, volcanic structures, and alluvial fan size and extent. The associated SAR imagery, which is sensitive to the surface roughness on the scale of the radar wavelength, provides information about the micro-topography of the surface. The combination of the two scales can be used to infer information about the surface geology such as the relative age of lava flows.

DATA DELIVERABLES

Data deliverables can be divided into three categories, pre-project deliverables, post-project deliverables, and map products including DEMs, imagery and other derived products. Depending on whether data is specifically collected to support a project or purchased from archived sources, not every deliverable category is applicable. The main goal of this chapter is to provide the DEM user with a list of the type of deliverables that may be available throughout the course of a project. Selection of those deliverables most useful for a particular project will depend on the type of data needed and the application.

Pre-Project Deliverables

Pre-project deliverables are designed to insure that the desired data is collected and will meet project accuracy and coverage requirements. Project planning, as covered earlier, is integral to the success of any project. Clear communication by appropriate pre-project deliverables can help the data provider and data user effectively communicate cost (and cost versus data quality tradeoffs), data quality expectations, data collection constraints, and schedule.

- A map (typically, U.S. Geological Survey maps are desirable for the purpose) showing the study area boundaries, flight paths and mapping swaths at a medium scale (1:50,000) or small scale (1:100,000).
- A shaded relief map of each swath indicating the area lost to layover, shadow or where the phase is unwrappable.
- A shaded relief composite mosaic of all the mapping swaths showing those gaps that will be filled in during the mosaicking process.
- A table giving the estimated amount and type of data voids on each swath and in the data mosaic must be provided.
- Documentation specifying altitude, airspeed, heading, start and end location, flight time, radar pulse spacing, bandwidth, center frequency and polarization, interferometer configuration (ping-pong or single antenna transmit), pulse width, and other flight and equipment information deemed appropriate. Maximal tolerance on flight or radar parameters before a line must be aborted should also be included.
- A schedule indicating expected date and time of flights, processing and data delivery dates.

Post-Project Deliverables

Post-project deliverables provide the DEM user with information about how closely the planned data collection objectives were met. Ancillary data may also include additional information about weather, ground control, or other pertinent data to facilitate use of the data in its intended application.

- An IFSAR data system report includes discussions of: data processing methods used both for strip map production and DEM mosaicking, sensor configuration parameters for each datatake, accuracy and precision of IFSAR data collected, accuracy of the topographic surface products, and any other data deemed appropriate.
- A flight report documents the mission date(s), time, flight altitude, airspeed, heading, start and end points of the data take, look angles to the near and far edge of the swath, radar mode parameters and any other information deemed pertinent. The report usually includes information about the aircraft motion including GPS derived flight information, INS data including attitude angles and attitude angle rates. Comparisons between planned and actual flight paths and radar parameters should be given with any deviations exceeding the maximal specified tolerances explicitly noted.
- A ground control report includes all the pertinent base station information and mission notes, including information on GPS station monument names and stability.
- A data processing report summarizes the parameters for processing the data and identifies any anomalies encountered during the processing.

Chapter 6

- A system calibration report indicates the time when and data used to calibrate the sensor for the project and an assessment of how accurately the sensor was calibrated.

Map Products
Map products are defined as any data deliverable that is derived from the IFSAR data. The range of products depends on the application and the amount of post processing done to the data. Most providers will accommodate a range of map projections, geoid choice, data format and delivery media to satisfy customer needs and requirements.

COST CONSIDERATIONS
The cost of IFSAR products depends on many factors. Some of the factors are accuracy, project size, geographic location, ground post spacing, terrain type and density, and type of the vegetation cover. Current reported prices for IFSAR generated DEMs are grouped into two categories: (1) project specific, where data is collected by the data provider to meet a specific customer mapping requirements, and (2) archival data where data is purchased from previously collected (and possibly processed) IFSAR mission data [Global Terrain Prices, 2001].

Project Specific
For project specific IFSAR, DEM prices range from $30/km^2 to $100/km^2 depending upon the site location, terrain ruggedness, foliage density and extracted vector data.

Archival Data
Archival data prices are lower than project specific prices and depend on whether the data must be reprocessed or can be used as previously processed. Archival data purchases are possible when the data collector, usually in exchange for a reduced collection and processing price, has reserved the data rights for a data collection. In affect, the data collector licenses the data to his client for a narrow use and retains distribution rights for all other uses. Data archive prices range from $11/km^2 to $25/km^2 for DEMs and $7/km^2 for IFSAR images. Table 6.8 shows a summary of prices for different postings and geographic locations.

Table 6.8 IFSAR X-band Prices.

Commercial X-Band Data Warehouse Prices			
Post Spacing(m)	Vertical RMSE(m)	Price Range per km^2	
		DEM	DEM and Image
5	1.0	$20-$100	$23-$110
10	1.5-2.0	$12-$55	$14-$60
10	2.0-3.0	$10-$45	$12-$50

TECHNOLOGICAL ADVANCEMENTS
A number of innovations in IFSAR technology and methodology are pressing toward finer resolutions and height accuracy, and improved characterization of the surface heights.

Airborne IFSAR systems continue to progress to finer resolutions and height acuity. At Ku band and other available bands, cm-scale resolutions are possible in the cross-track direction. In azimuth, spotlight mode processing can achieve sub-meter resolutions. Experimental systems by Sandia and ERIM have demonstrated this capability. With such fine resolution, it is straightforward to achieve relative accuracy that is sub-meter because of the large amount of averaging that is possible.

The challenge for future systems is unambiguously differentiating the heights of the various physical surfaces on the ground, from treetop to bare earth. Systems such as GeoSAR, with X- and P-band interferometry and dual-polarization, are the first attempt to address this issue [Hensley et al, 2001]. In the future, we expect to see fully polarimetric interferometers, possibly at multiple frequencies, as the next technological leap. Scattering from randomly oriented objects like leafy canopies tends to randomize the polarization of the electromagnetic signal, while scattering from tree-trunks and sloped surfaces has a more deterministic effect on the polarization. With the full polarization matrix available, scattering from treetops can be separated from surface interactions [Cloude and Papathanassiuo, 1997]. With interferometric polarimetry, it is then possible to assign a height to the treetops and to the surface independently. This is an active area of research, however no systems have been built as polarimetric interferometers at sufficient accuracy to quantify the performance of the concepts.

Numerous space mission concepts to produce global topography beyond the level attained by SRTM have been forwarded to NASA and the Department of Defense, but none have yet been funded by these agencies. Some of these proposed missions were to have two spacecraft orbiting in formation with precise inter-craft metrology systems and with the radar operating at L-band frequencies. Others proposed to configure a boom with dual apertures to form the interferometer, and with the radar operating at the higher frequencies. The proposed cost of these missions was high, and can only be justified in terms of global map production. While the need for targeted accurate topography worldwide is well-established, the need for global maps has been insufficient to justify the cost.

Several nations, however, following an innovative concept proposed by D. Massonnet of CNES, are considering a new SAR constellation known as an interferometric cartwheel [Massonnet, 2001]. In this concept, a standard orbiting SAR serves as a signal source for an interferometer. Several receive-only satellites orbit in phased, elliptical orbits such that, in the frame of the mean circular orbit, the satellites execute epi-cyclic motion around an ellipse once per orbit. These receive-only satellites act as the interferometer apertures, with baseline lengths highly variable in time. The baselines are typically several kilometers, so the height acuity is excellent. Though the antennas are very small compared to standard SAR antennas, to reduce cost, it can be shown that the usual performance degradation one would expect due to ambiguities are greatly reduced when the baseline is long. Planners expect to be able to generate global topography in about 1 year of mapping at 1 m accuracy at a resolution determined by the signal source, but enhanced by super-resolution techniques. The first demonstration experiments are expected in the next few years, when the details of baseline metrology and calibration will be examined. Operational systems may arise in about a decade.

Topography can change on very rapid time scales, so there is a continuing need to update topographic maps, particularly at the finest resolutions and accuracy. Future systems may map topographic change as it evolves from the vantage point of geosynchronous orbit. Topographic change mapping using IFSAR can be done when either the interferometric baseline is zero, or the base topography is known and can be removed from the interferometry data. Any change in the range from the radar to the surface can be mapped at the millimeter scale. From geosynchonous orbit, the baselines will be very small, and topographic change can be measured from hour to hour as the system continuously points at a site of interest.

AUTHOR BIOGRAPHIES

The principal author for this chapter is Scott Hensley, Radar Science and Engineering Section, Jet Propulsion Laboratory, 4800 Oak Grove Drive, Pasadena, California 91109. Contributing authors to this Chapter are Riadh Munjy from Earth Data International, Inc., and Paul Rosen from the Jet Propulsion Laboratory.

Scott Hensley received his BS degrees in Mathematics and Physics from the University of California at Irvine. He received a PhD in Mathematics from the State University of New York at

Stony Brook where he specialized in the study of differential geometry. Hensley is currently a Principal Engineer and GeoSAR Project Manager at the Jet Propulsion Laboratory. He has developed processors for both airborne and spaceborne interferometric applications and leads the processor development activity for the GeoSAR program. Current research includes studying the amount of penetration into the vegetation canopy using GeoSAR data as well as simultaneous L and C band TOPSAR measurements and repeat pass airborne interferometry data collected at lower frequencies. He was the technical lead of the SRTM Interferometric Processor Development Team.

Riadh Munjy is Professor of Geomatics Engineering at California State University, Fresno. He is also the chief scientist at Earth Data International, Inc. working on the development of the GeoSAR System. He has over 30 years of experience in mapping. Munjy obtained his BSc in Civil Engineering from the University of Baghdad, Iraq in 1976 and MS in applied mathematics, MSCE and PhD in Civil Engineering from the University of Washington , Seattle respectively in 1978, 1980 and 1982.

Paul Rosen is supervisor of the Interferometric Synthetic Aperture Radar Algorithms and System Analysis Group at the Jet Propulsion Laboratory, and visiting faculty member and lecturer at the California Institute of Technology. Rosen's assignments at JPL include independent scientific and engineering research in methods and applications of interferometric SAR. He has developed interferometric SAR processors for airborne topographic mapping systems such as the JPL TOPSAR and ARPA IFSARE, space-borne topographic and deformation processors for sensors such as ERS, JERS, RadarSAT, and the Shuttle Radar Topography Mission (SRTM). Rosen is the Project Element Manager for the development of topography generation algorithms for SRTM. He has also led several proposals for surface deformation satellite missions.

REFERENCES

Ackermann, F., 1994. Digital elevation models - techniques and application, quality standards, development, *International Archives of Photogrammetry and Remote Sensing*, 30(4): 421-432.

Bamler, R., and P. Hartl, 1998. Synthetic aperture radar interferometry, *Inverse Problems*, 14, R1-54.

Burrough, P.A., 1986. *Principles of Geographical Information Systems for Land Resources Assessment*, Oxford University Press, Oxford.

Cloude, S.R., and K.P. Papathanassiou, 1997. Polarimetric optimization in radar interferometry, *Electronics Letters*, 33(13): 1176-1178.

Curlander, J.C., and R.N. McDonough, 1991. *Synthetic Aperture Radar Systems and Signal Processing*, Wiley-Interscience.

Elachi, C., 1998. *Spaceborne Radar Remote Sensing: Applications and Techniques*, IEEE Press, New York, NY.

Farr, T., and M. Kobrick, 2000. Shuttle radar topography mission produces a wealth of data, *EOS, Trans. of American Geophys. Union,* 81(48): 583-585.

Franceschetti, G., and R. Lanari, 1999. *Synthetic Aperture Radar*, CRC Press.

Galy, H.M., and R.A. Sanders, 2000. Using SAR imagery for flood modeling, *RGS-IBG Annual Conference Prec.*

Global Terrain Prices, 2001. URL: http://www.globalterrain.com.

Goldstein, R.M., 1995. Atmospheric limitations to repeat-track radar interferometry, *Geophys. Res. Lett.*, 22, 2517-2520.

Graham, L.C., 1974. Synthetic interferometric radar for topographic mapping," *Proc. IEEE*, 62(6): 763-768.

Gray, A.L., and P.J. Farris-Manning, 1993. Repeat-pass interferometry with an airborne synthetic aperture radar, *IEEE Trans. Geosci. Rem. Sens.*, 31(1): 180-191, 1993.

Hagberg, J.O., L.M.H. Ulander, and J. Askne, 1995. Repeat-pass SAR interferometry over forested terrain, *IEEE Trans. Geosci. Rem. Sens.*, 33(2): 331-340.

Hensley, S., and F.H. Webb, 1994. Comparison of Long Valley TOPSAR data with kinematic GPS measurements, *IGARSS Proceedings*, Pasadena, CA.

Hensley, S., J. Klein, P.A. Rosen, E. Chapin, S.N. Madsen, and F.H. Webb, 1995. Repeat pass aircraft interferometry results at Portage Lake, Maine, and Innisfail, Australia, *Proc. of the AIRSAR Sci. Workshop.*

Hensley, S., E. Chapin, A. Freedman, C. Le, S. Madsen, T. Michel, E. Rodriguez, P. Siqueira, and K. Wheeler, 2001. First P-band results using GeoSAR mapping system, *Proceedings of IGARSS 2001*, Sydney, Australia.

Hokeman, D., and C. Varekamp, 2001. Observation of tropical rain forest trees by airborne high-resolution interferometric radar, *IEEE Trans. Geo. Sci, Rem. Sen*., 39(3).

Kovaly, J., 1976. *Synthetic Aperture Radar*, Artech House Inc., Boston, MA.

Leberl, F.W., 1990. *Radargrammetric Image Processing*, Artech House Inc., Boston, MA.

Lewis, A.J., and F.M. Henderson, 1999. Radar fundametals: The geoscience perspective, in *Manual of Remote Sensing*, Artech House Inc., Boston, MA, 3(3).

Li, F., and R.M. Goldstein, 1990. Studies of multibaseline spaceborne interferometric synthetic aperture radar, *IEEE Trans. Geosci. Remote Sensing*, 28: 88-97.

Madsen, S.N., H.A. Zebker, and J. Martin, 1993. Topographic mapping using radar interferometry: Processing techniques, *IEEE Trans. Geosci. and Rem. Sens.*, 31(1): 246-256.

Madsen, S.N., N. Skou, J. Granholm, K.W. Woelders, and E.L. Christensen, 1996. A system for airborne SAR interferometry, *Intl. J. Elect. Comm.*, 50(2): 106-111.

Madsen, S.N., and H.A. Zebker, 1999. Synthetic aperture radar interferometry: Principles and applications, in *Manual of Remote Sensing*, Artech House Inc., Boston, MA, 3(6).

Madsen, S.N., J.M. Martin, and H.A. Zebker, 1993. Analysis and evaluation of the NASA/JPL TOPSAR across-track interferometric SAR system, *IEEE Trans. Geosci. Rem. Sens*., 33()2): 383-391.

Massonnet, D., 2001. Capabilities and limitations of the interferometric cartwheel, *IEEE Trans. Geo. Sci, Rem. Sen*., 39(3).

Mercer, J.B., and M. Gill, 1998. Radar-derived DEMs for yrban areas, *Proceedings of the ISPRS Commission IV Symposium,* Stuttgart, Germany.

Mercer, J.B., J. Bryan, and S. Schnick, 1999. Comparison of DEM from Star3i and scanning laser, *ISPRS Commission III Workshop*, La Jolla, CA.

Positional Accuracy Handbook*,* October, 1999, Minnesota Planning Land Management Information Center, URL: http://www.fgdc.gov/standards/status/sub1_3.html.

Raney, K., 1999. Radar fundamentals: Technical perspective," in *Manual of Remote Sensing*, Artech House Inc., Boston, MA, 3(2).

Real, C., R.I. Wilson, and T.P. McCrink, 1997. Suitability of airborne-radar topographic data for evaluating earthquake-induced ground failure hazards, *12th Int. Conf. on Appl. Geol. Rem. Sens.*, Denver, CO.

Rodriguez, E., T. Michel, D. Harding, and J.M. Martin, 1999. Comparison of airborne InSAR-derived heights and laser altimetry, *Radio Science,* in press.

Rodriguez, E., J.M. Martin, and T. Michel, 1999. Classification studies using Interferometry, *Radio Science*, in press.

Rodriguez, E., C. Morris, E. Belz, 2006. A global assessment of the SRTM performance*, Photogrammetric Engineering and Remote Sensing*, 72(3): 249-260.

Rodriguez, E., C. Morris, E. Belz, E. Chapin, J. Martin, W. Daffer, and S. Hensley, 2005. An assessment of the SRTM topographic products, Technical Report JPL D-31639, Jet Propulsion Laboratory, Pasadena, CA.

Rogers, A.E.E., and R.P. Ingalls, 1969. Venus: Mapping the surface reflectivity by radar interferometry," *Science*, 165: 797-799

Rosen, P.A., S. Hensley, I.R. Joughin, F.K. Li, S. Madsen, E. Rodriguez, and R.M. Goldstein, 2000. Synthetic aperture radar interferometry, *IEEE Proc*., 88(3).

Schwäbisch, M., and J. Moreira, 1999. The high resolution airborne interferometric SAR AeS-1, *Proceedings of the 4th International Airborne Remote Sensing Conference and Exhibition*, Ottawa, Canada.

Slater, J., G. Garvey, J. Haase, B. Heady, G. Kroenung, J. and Little, 2006. The SRTM data finishing process and products, Photogrammetric Engineering and Remote Sensing, 72(3): 237-247.

Sos, T.G., H.W. Kilmach, and G.F. Adams, 1994. High performance interferometric SAR description and capabilities, *Proceedings of Tenth Thematic Conference on Geologic Remote Sensing*, San Antonio, TX, 2.

Tarayre, H., and D. Massonnet, 1996. Atmospheric propagation heterogeneities revealed by ERS-1 interferometry, *Geophys. Res. Lett.*, 23(9): 989-992.

Tennant, J.K., and T. Coyne, 1999. STAR-3I Interferometric Synthetic Aperture Radar (INSAR): Some lessons learned on the road to commercialization, *Proc. of the Fourth Intl. Airborne Rem. Sens. Conference and Exhibition/ 21st Canadian Symposium on Remote Sensing*, Ottawa, Ontario, Canada.

Zebker, H.A., and R.M. Goldstein, 1986. Topographic mapping from interferometric SAR observations, *J. Geophys. Res.*, 91: 4993-4999.

Zebker, H.A., S.N. Madsen, J. Martin, K.B. Wheeler, T. Miller, Y. Lou, G. Alberti, S. Vetrella, and A. Cucci, , 1992. The TOPSAR interferometric radar topographic mapping instrument, *IEEE Trans. Geosci. Remote Sensing*, 30.

Zebker, H.A., and J. Villasenor, 1992. Decorrelation in interferometric radar echoes, *IEEE Trans. Geosci. Rem. Sens.*, 30: 950-959.

Zebker, H.A., T.G. Farr, R.P. Salazar, and T.H. Dixon, 1994. Mapping the world's topography using radar interferometry - the TOPSAT mission, *Proc. IEEE*, 82(12): 1774-1786.

Zebker, H.A., C.L. Werner, P.A. Rosen, and S. Hensley, 1994. Accuracy of topographic maps derived from ERS-1 interferometric radar, *IEEE Trans. Geosci. Rem. Sens.*, 32: 823-836.

Zebker, H.A., P.A. Rosen, and S. Hensley, 1997. Atmospheric effects in interferometric synthetic aperture radar surface deformation and topographic maps, *J. Geophys. Res.*, 102, 7547-7563.

Zisk, S.H., 1972. A new Earth-based radar technique for the measurement of lunar topography, *Moon*, 4: 296-300.